Supporting Information

Synthesis and characterization of group (IV) metal alkoxide complexes containing imine based bis-bidentate ligands: Effective catalysts for the ring opening polymerization of lactides, epoxides and polymerization of ethylene

Sagnik Kumar Roymuhury,[†] Debashis Chakraborty,[†,] and Venkatachalam Ramkumar[‡]*

[†]Department of Chemistry, Indian Institute of Technology Patna, Patna-800 013, Bihar, India

[‡]Department of Chemistry, Indian Institute of Technology Madras, Chennai-600 036, Tamil Nadu, India

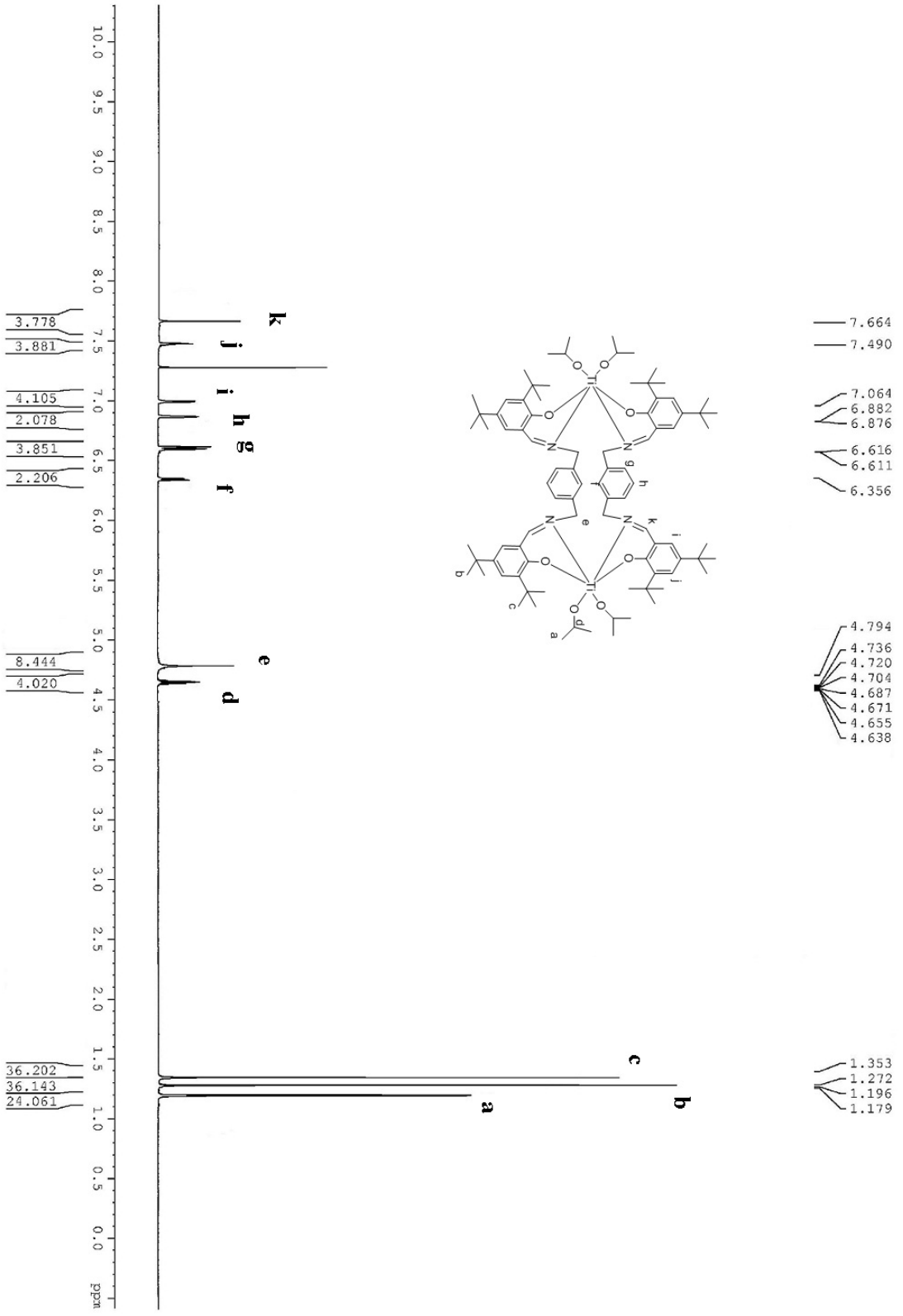

Figure S1.[1]H NMR (400 MHz, $CDCl_3$) of Compound **1**

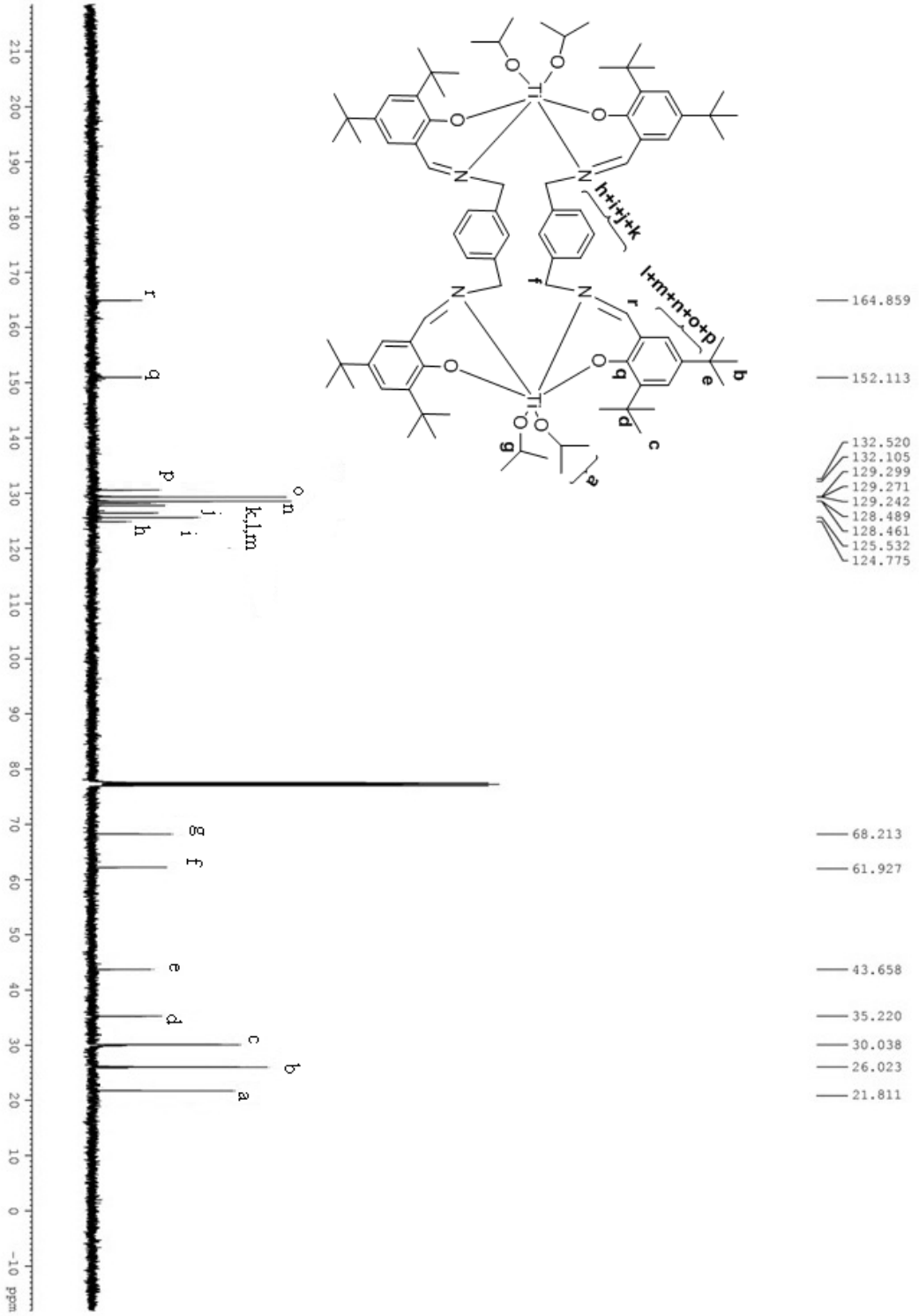

Figure S2. ^{13}C NMR (100 MHz, $CDCl_3$) of Compound **1**

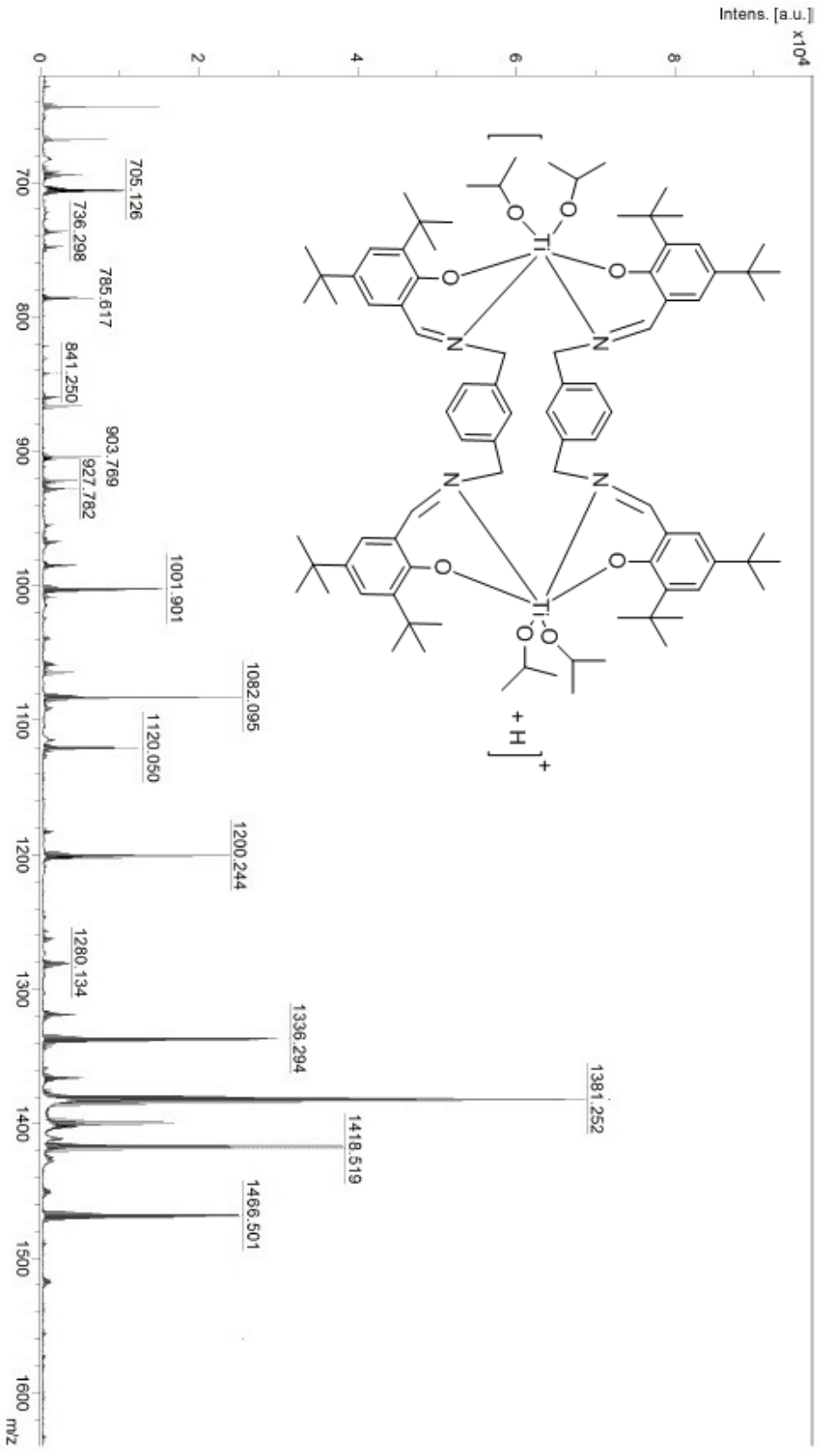

Figure S3.MALDI-TOF mass spectrum of Compound **1**

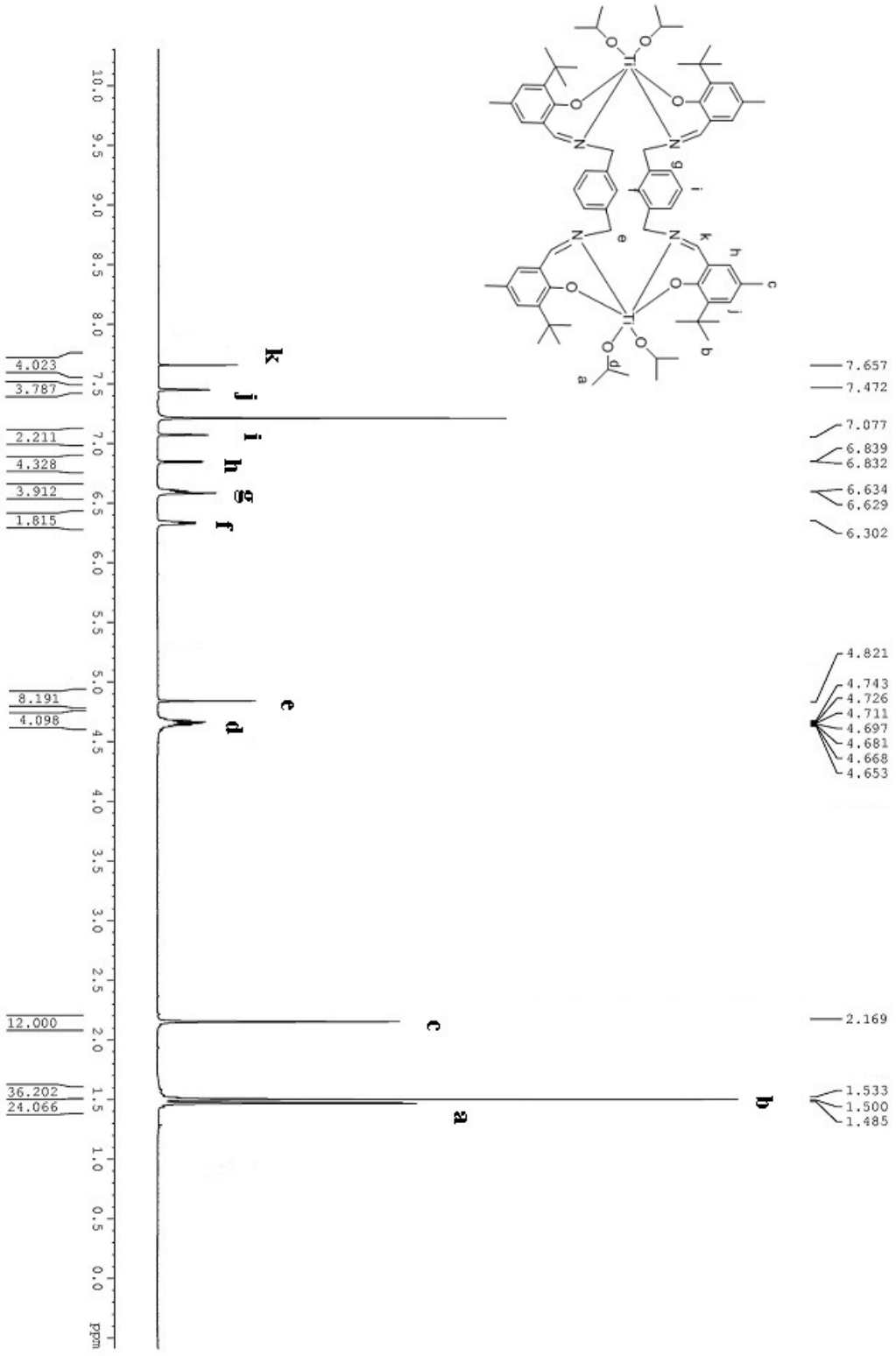

Figure S4. ^{1}H NMR (400 MHz, $CDCl_3$) of Compound **2**

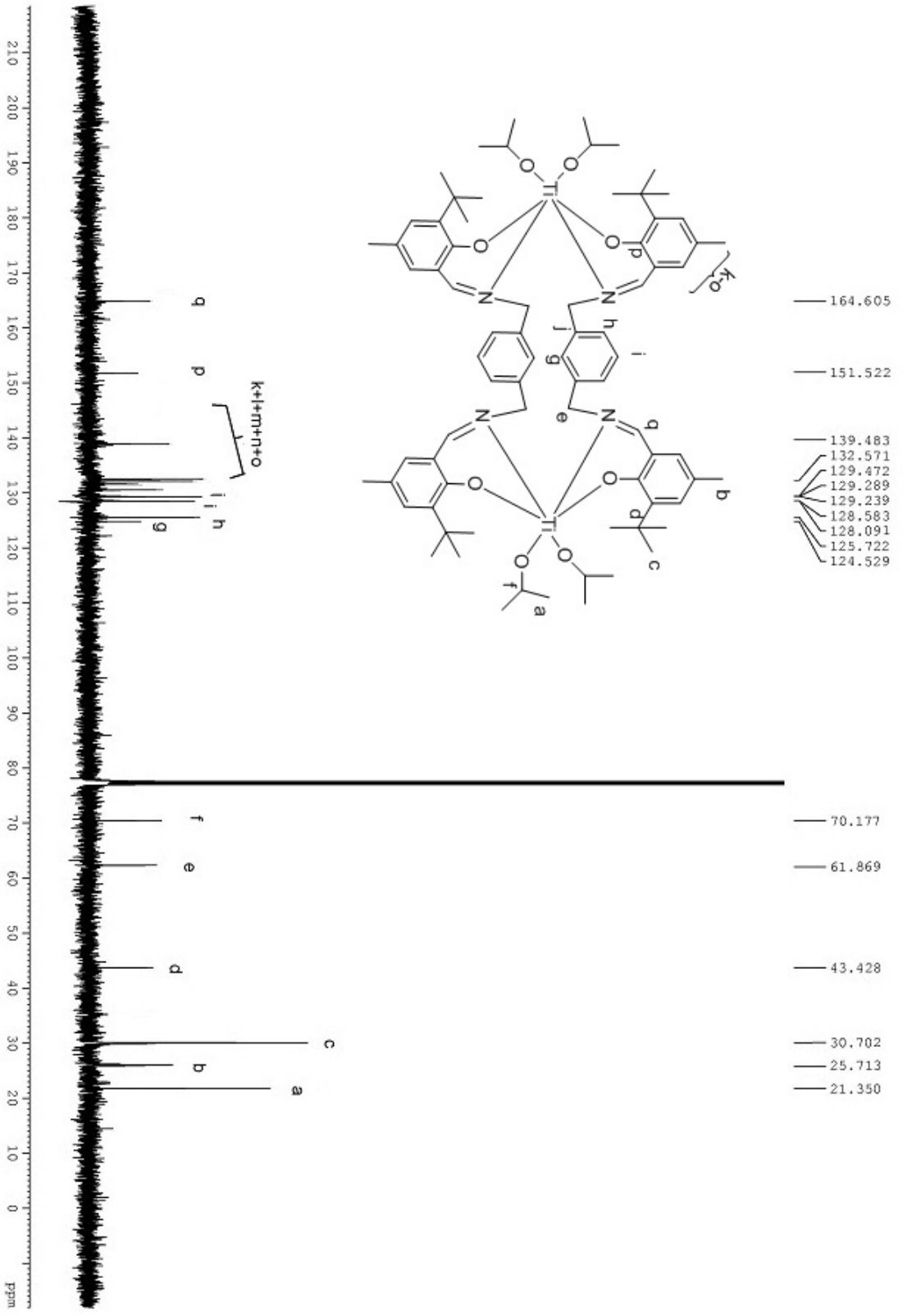

Figure S5. ^{13}C NMR (100 MHz, $CDCl_3$) of Compound **2**

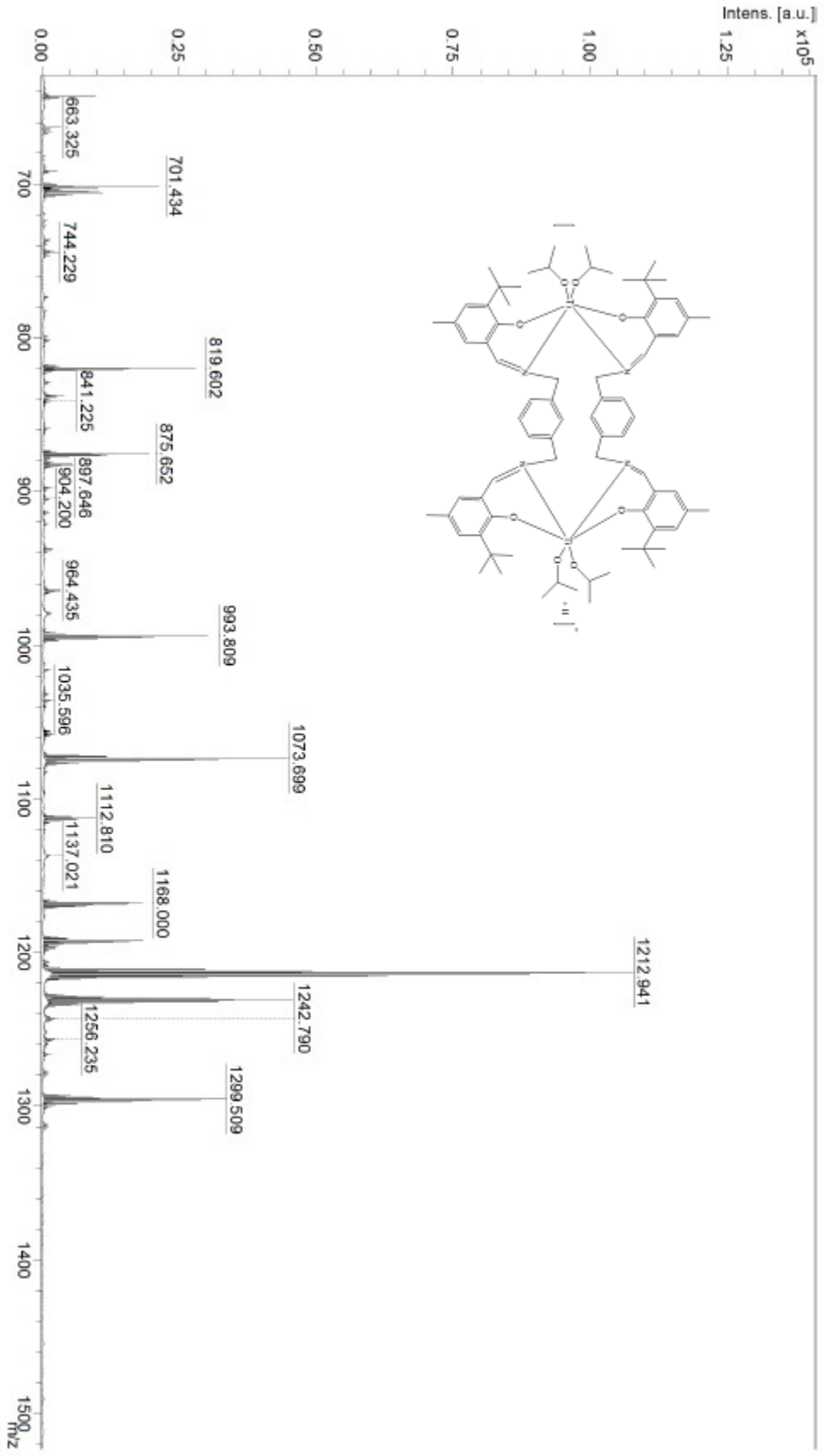

Figure S6.MALDI-TOF mass spectrum of Compound **2**

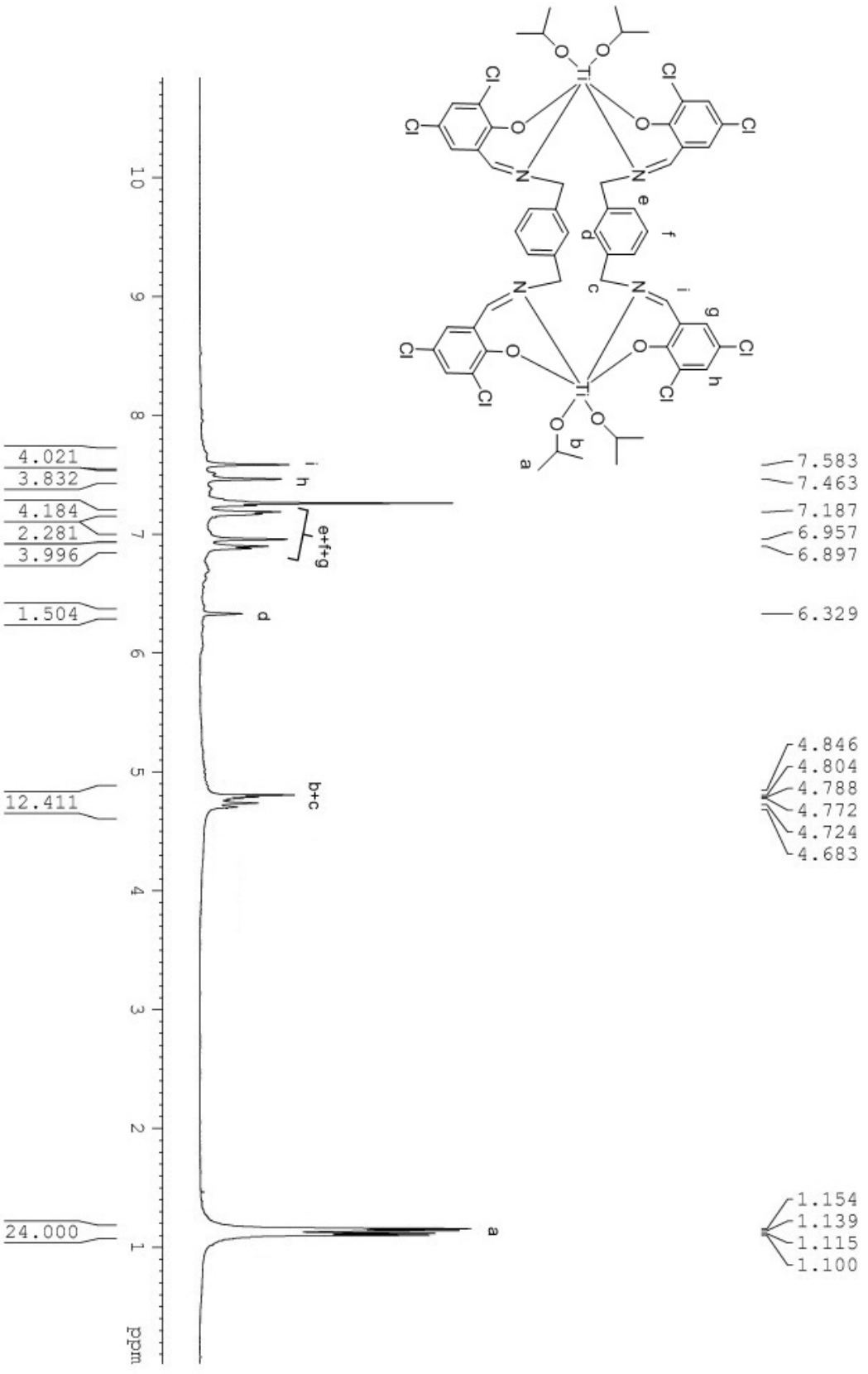

Figure S7.[1]H NMR (400 MHz, $CDCl_3$) of Compound **3**

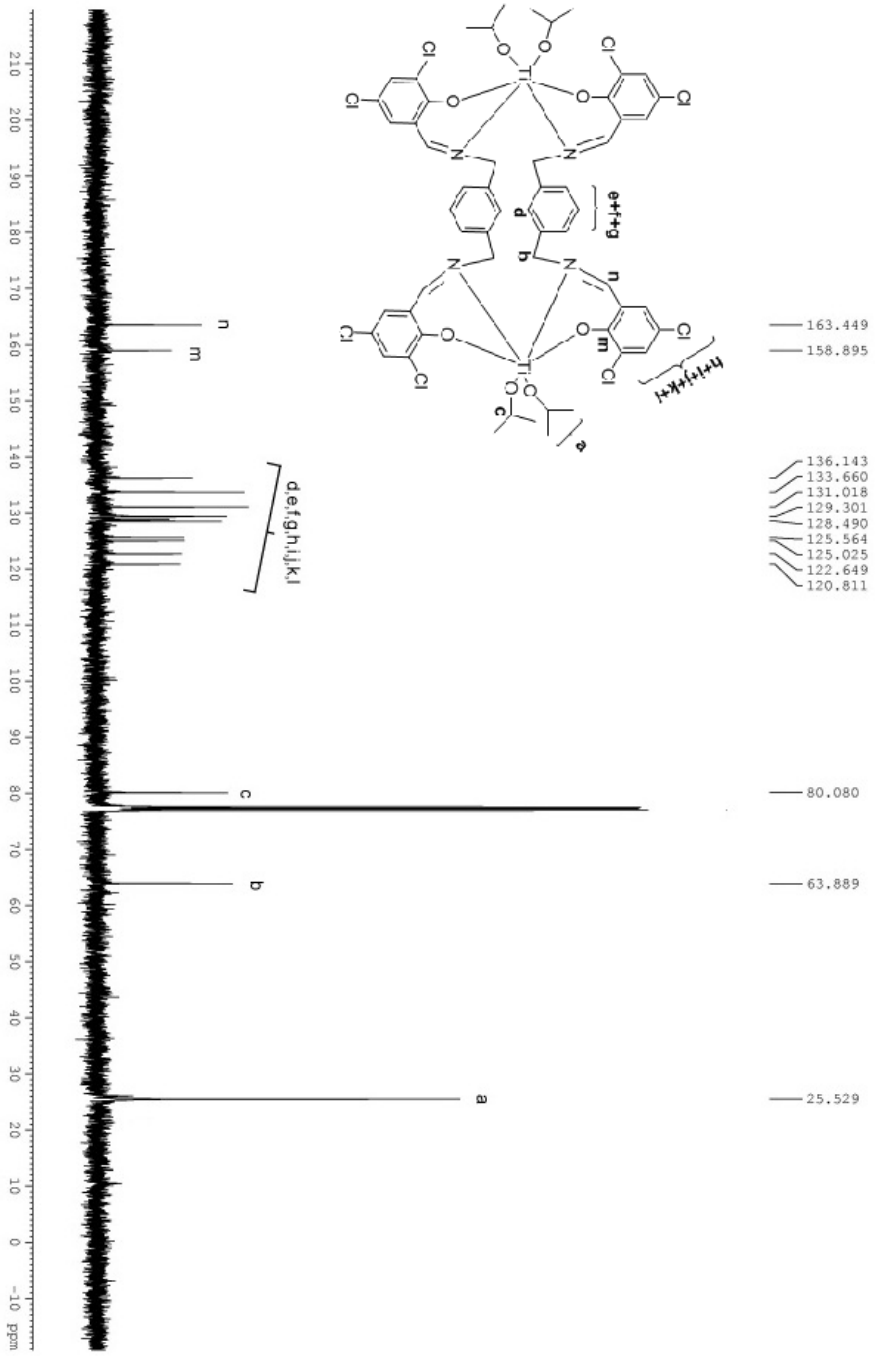

Figure S8. ^{13}C NMR (100 MHz, $CDCl_3$) of Compound **3**

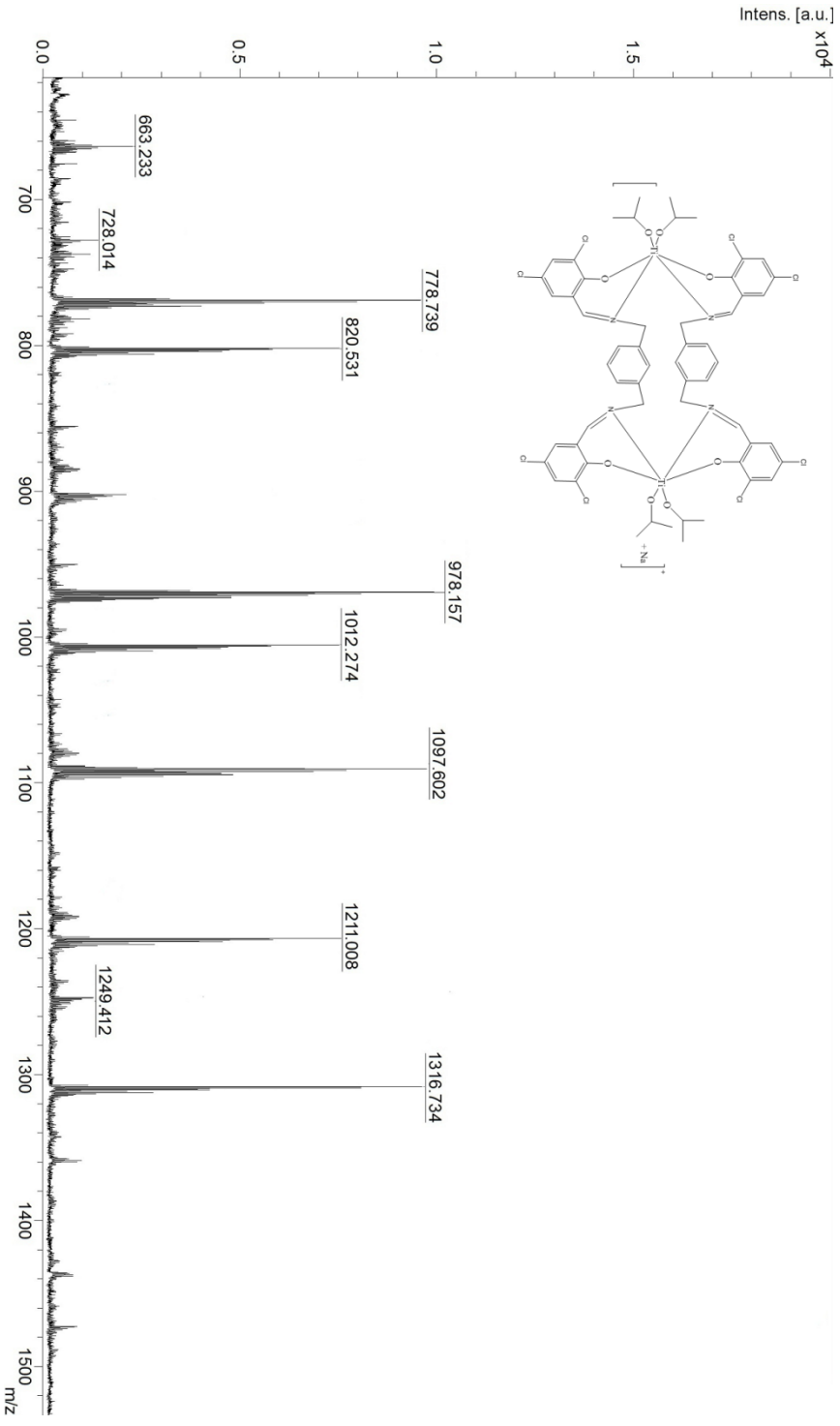

Figure S9.MALDI-TOF mass spectrum of Compound **3**

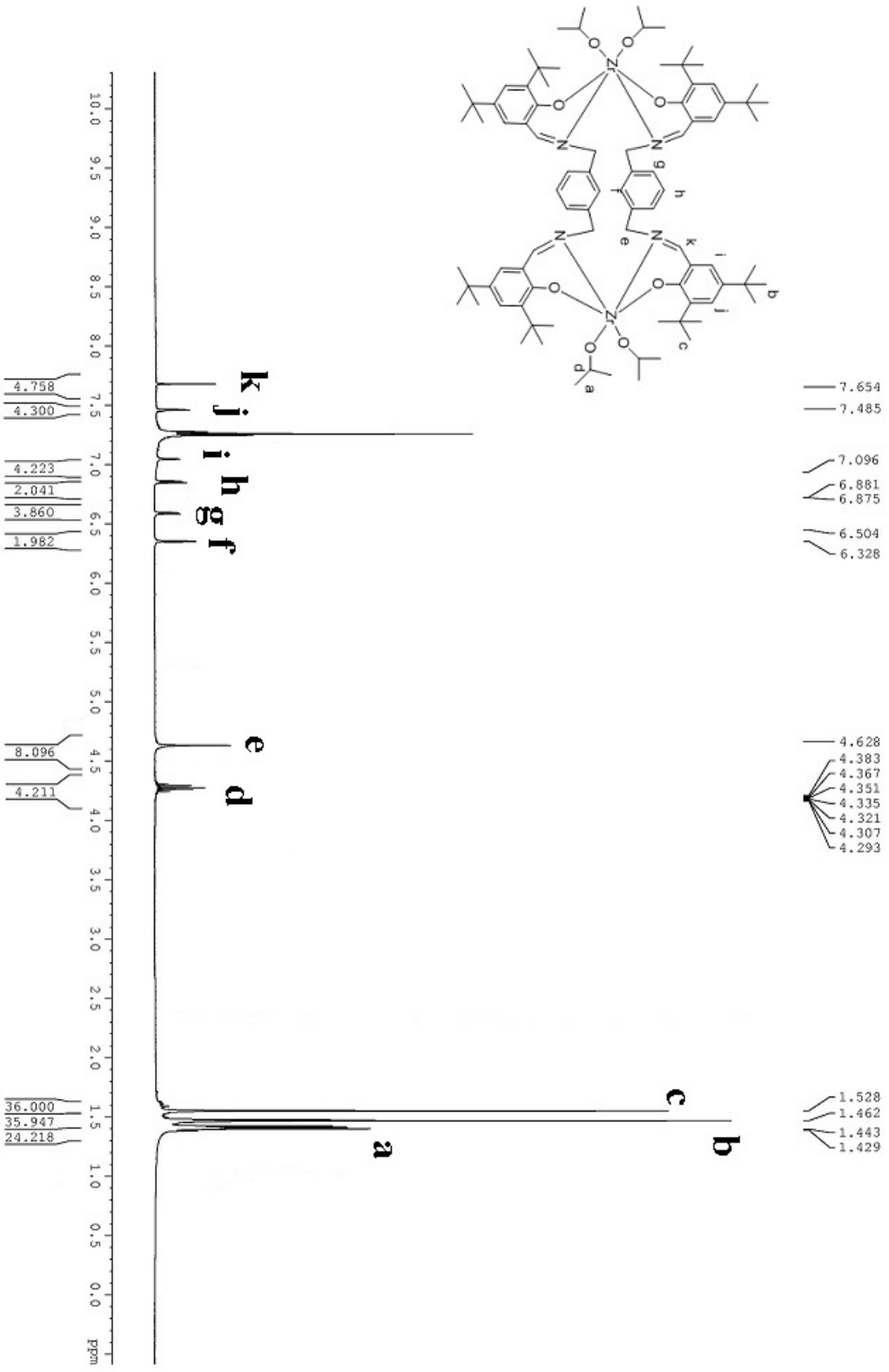

Figure S10.[1]H NMR (400 MHz, $CDCl_3$) of Compound **4**

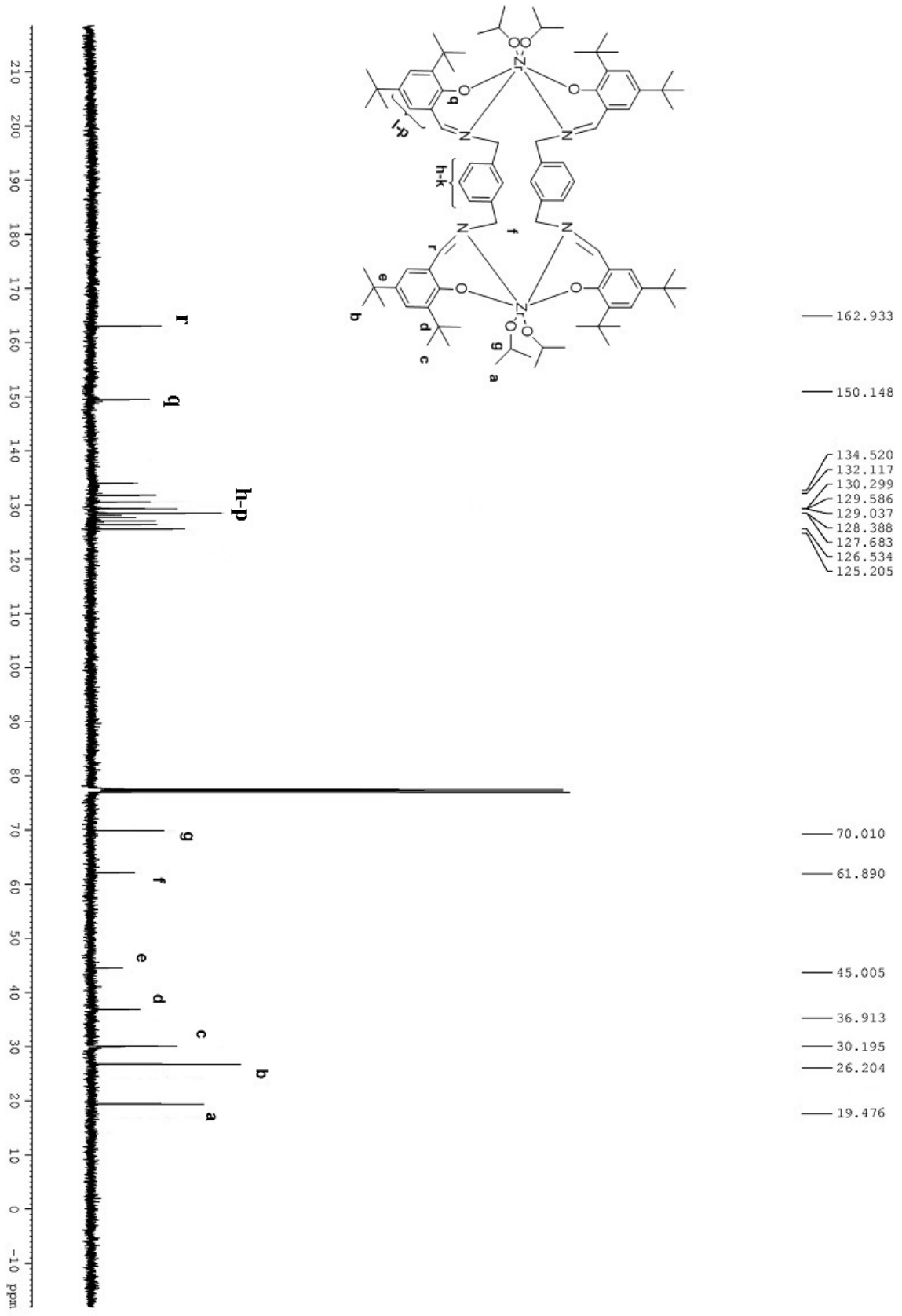

Figure S11. ^{13}C NMR (100 MHz, $CDCl_3$) of Compound **4**

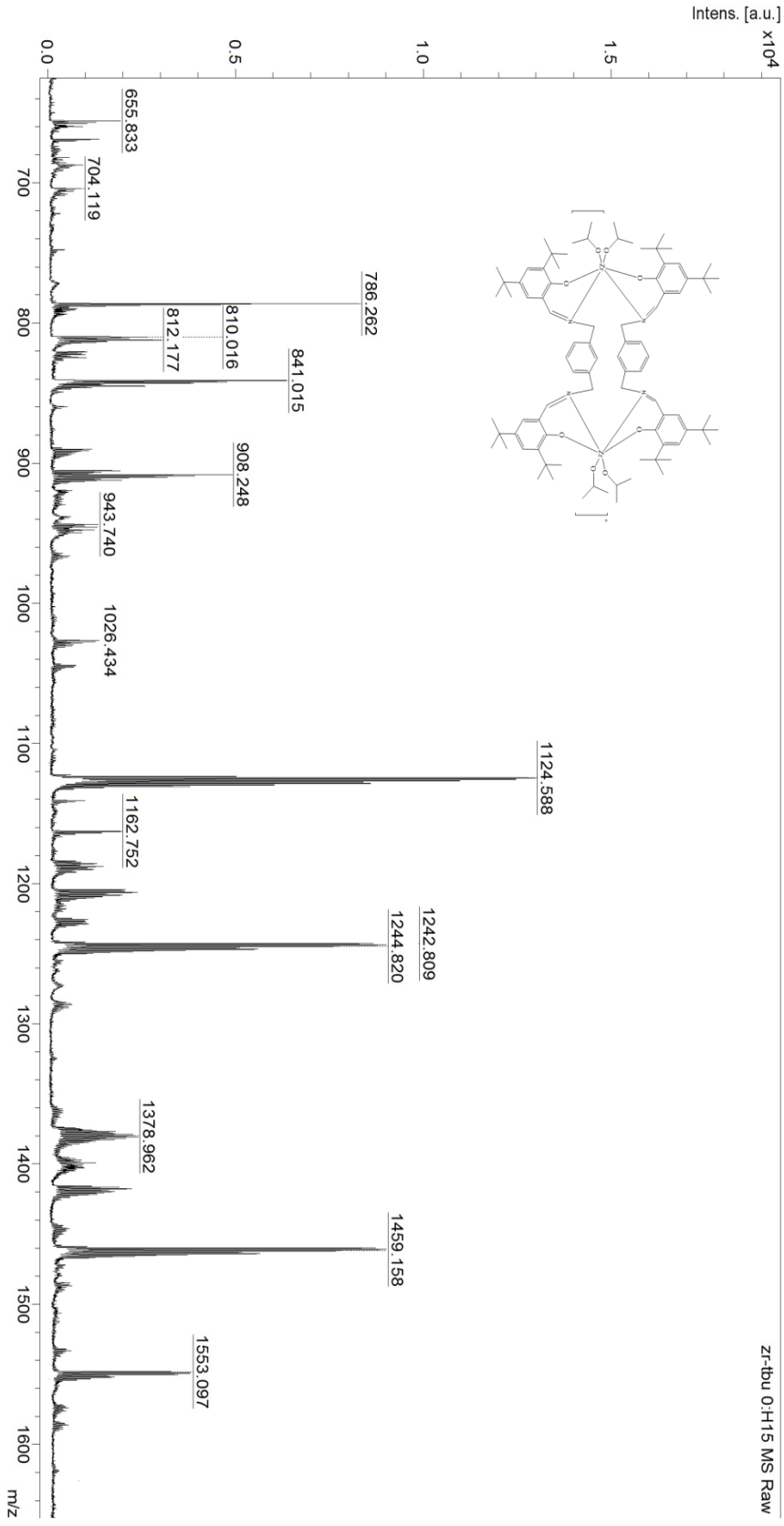

Figure S12.MALDI-TOF mass spectrum of Compound **4**

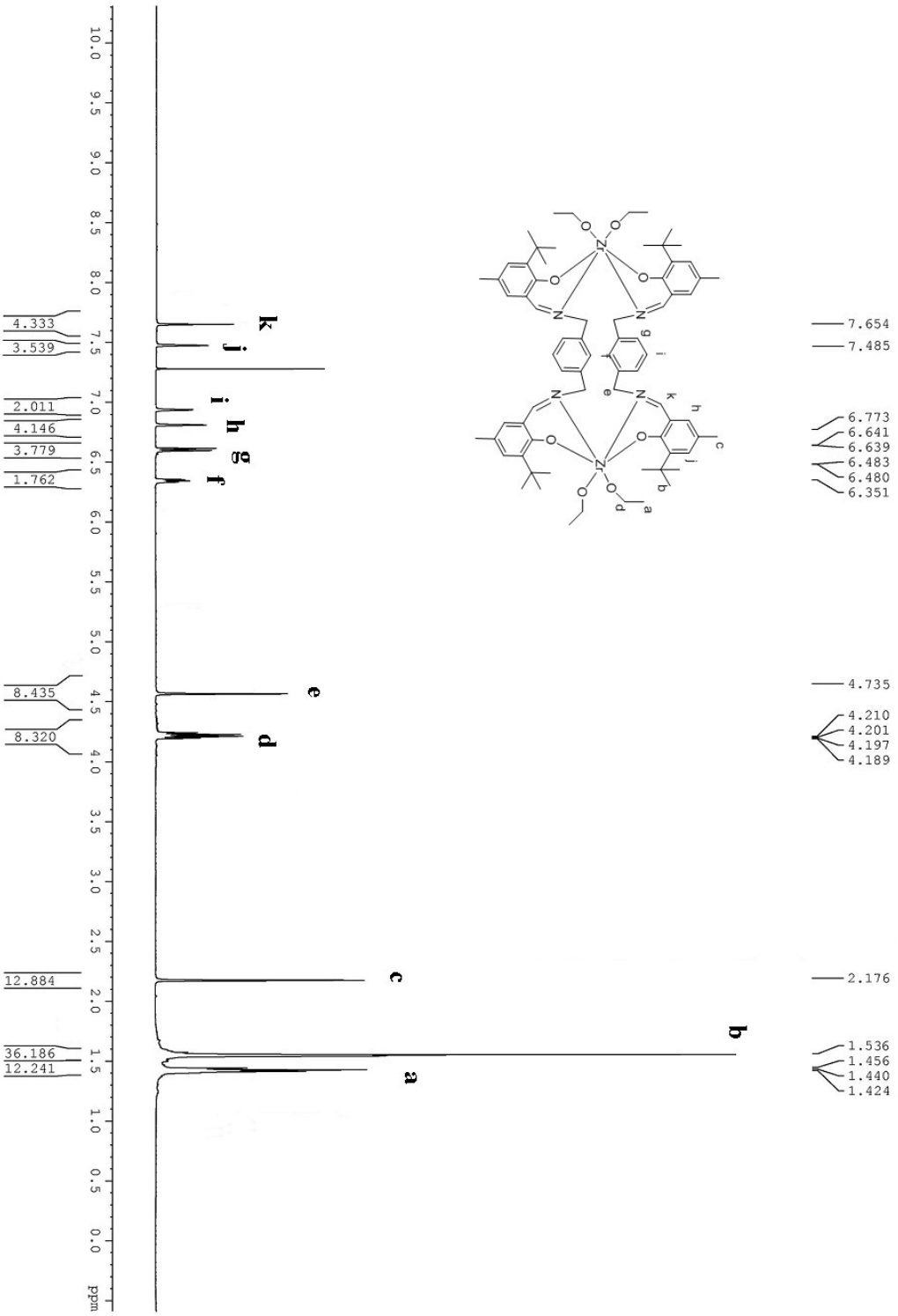

Figure S13. ^{1}H NMR (400 MHz, $CDCl_3$) of Compound **5a**

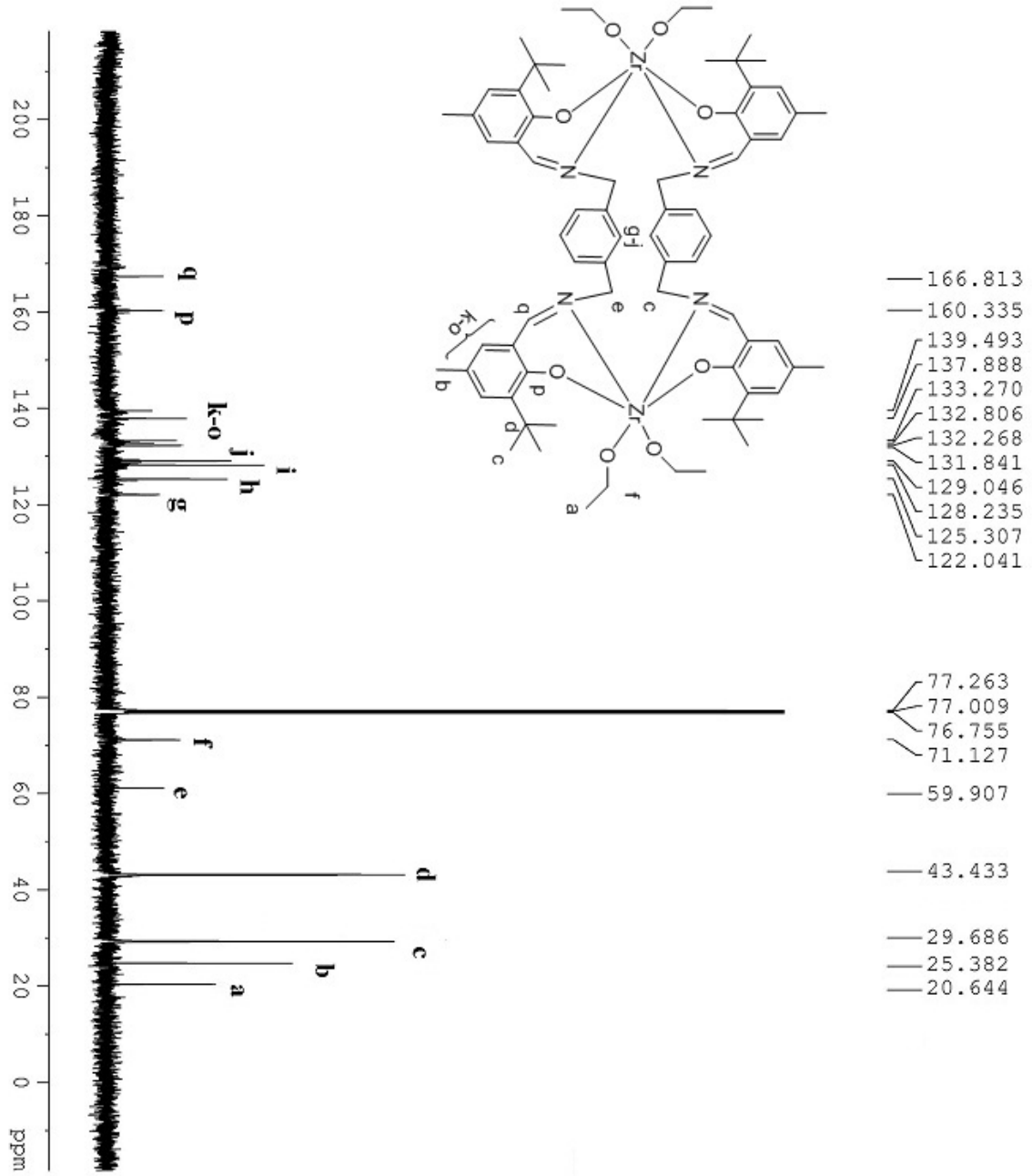

Figure S14. ^{13}C NMR (100 MHz, $CDCl_3$) of Compound **5a**

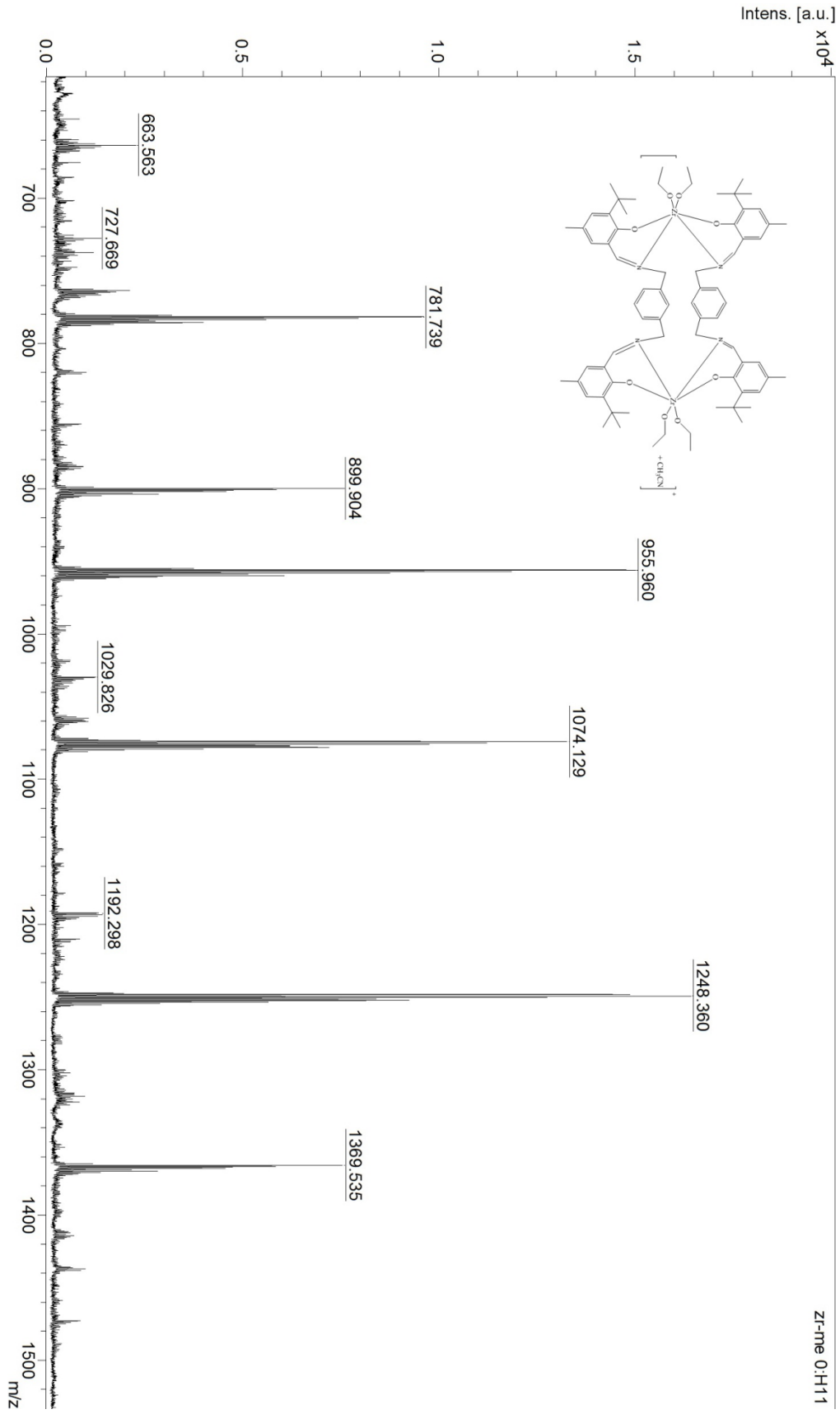

Figure S15.MALDI-TOF mass spectrum of Compound **5a**

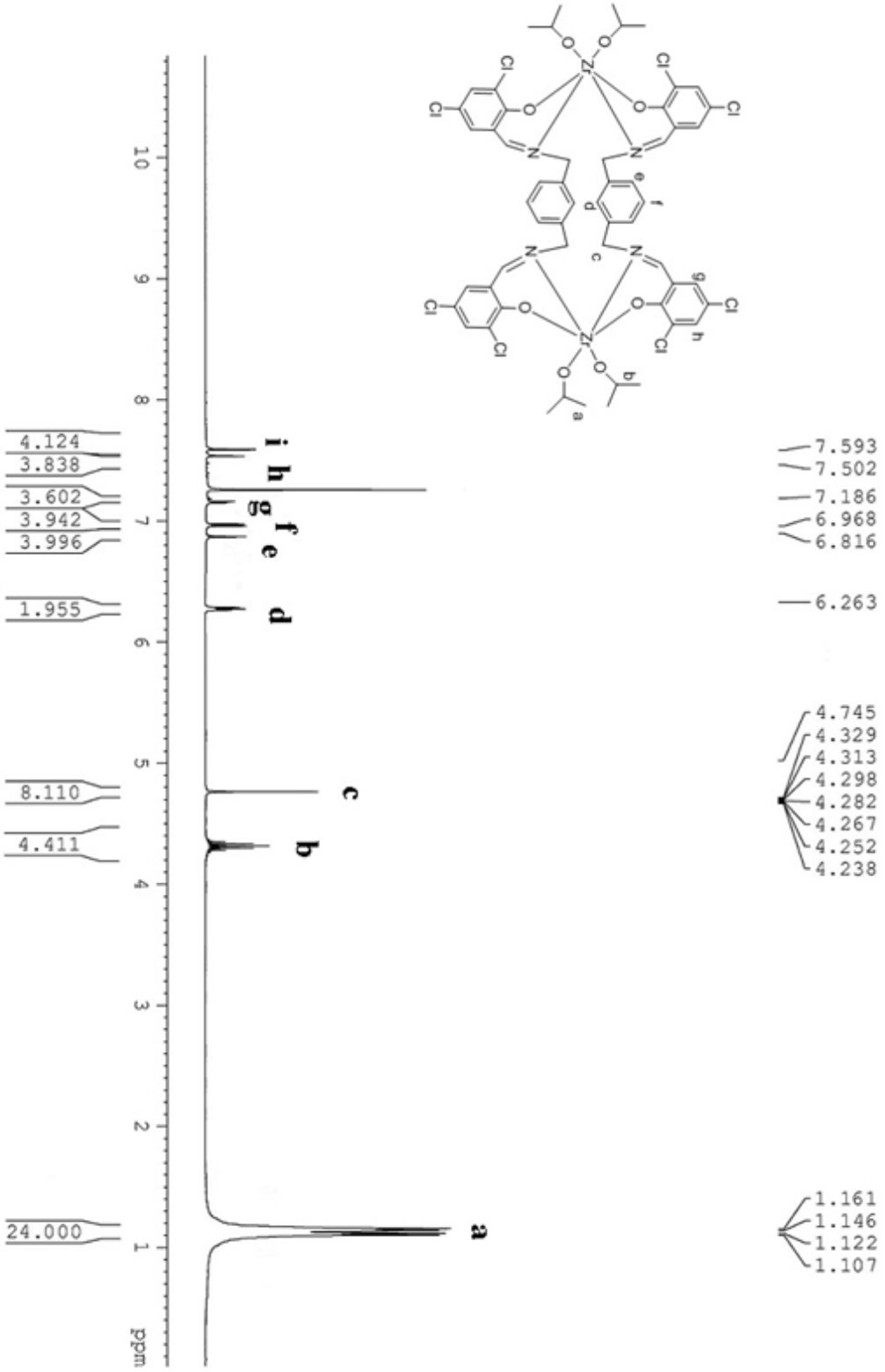

Figure S16. ^{1}H NMR (400 MHz, $CDCl_3$) of Compound **6**

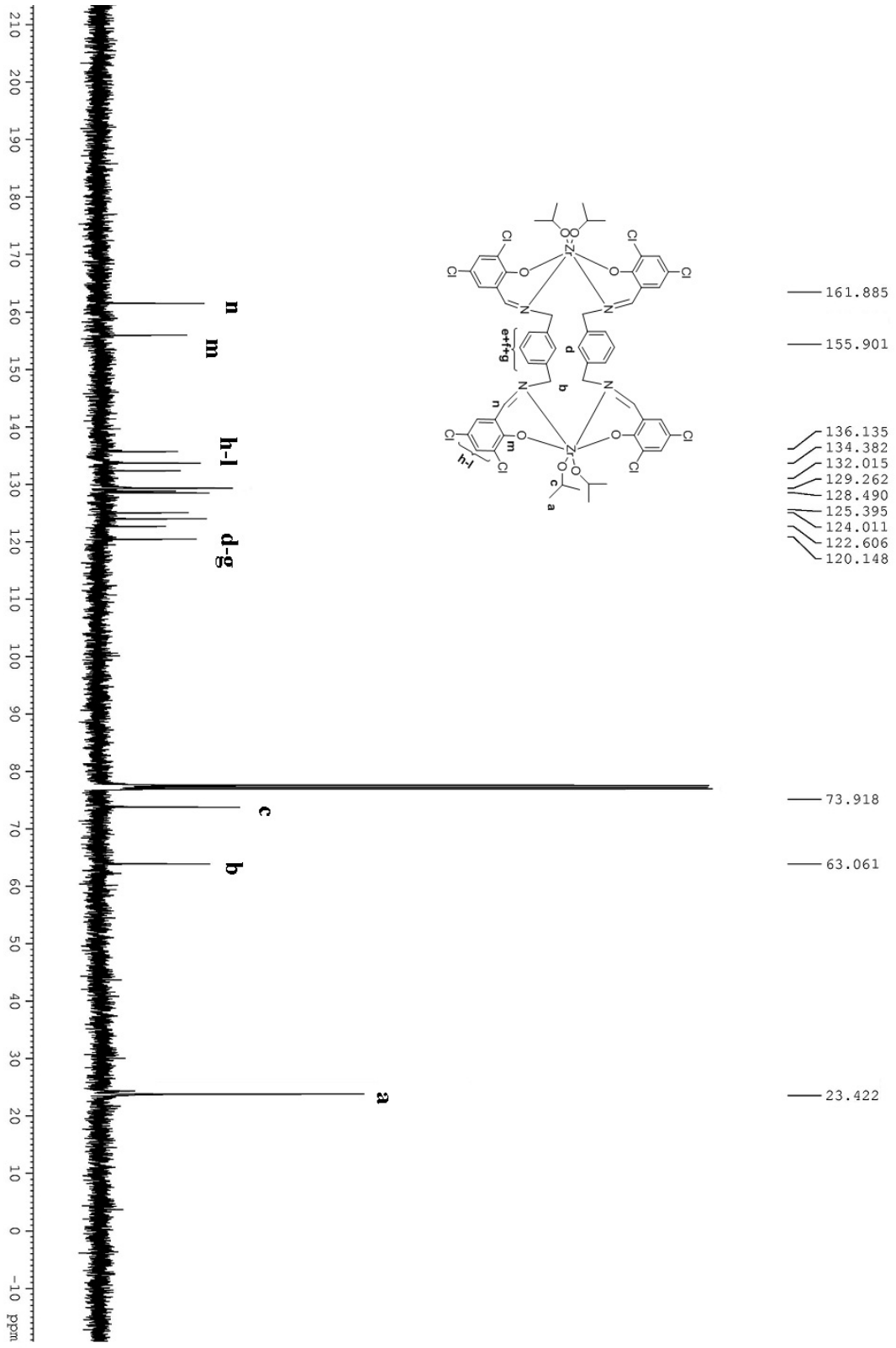

Figure S17. ^{13}C NMR (100 MHz, $CDCl_3$) of Compound **6**

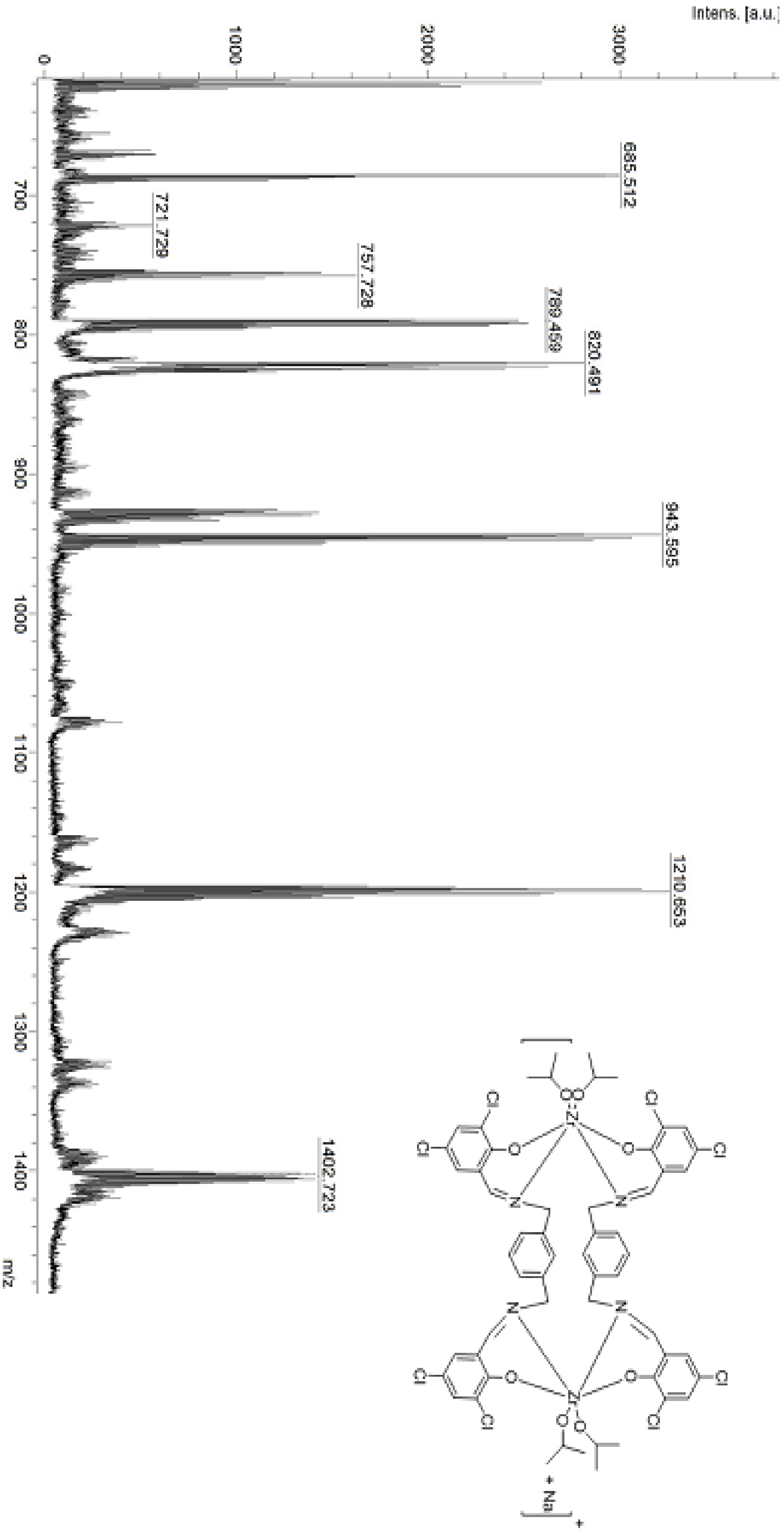

Figure S18.MALDI-TOF mass spectrum of Compound **6**

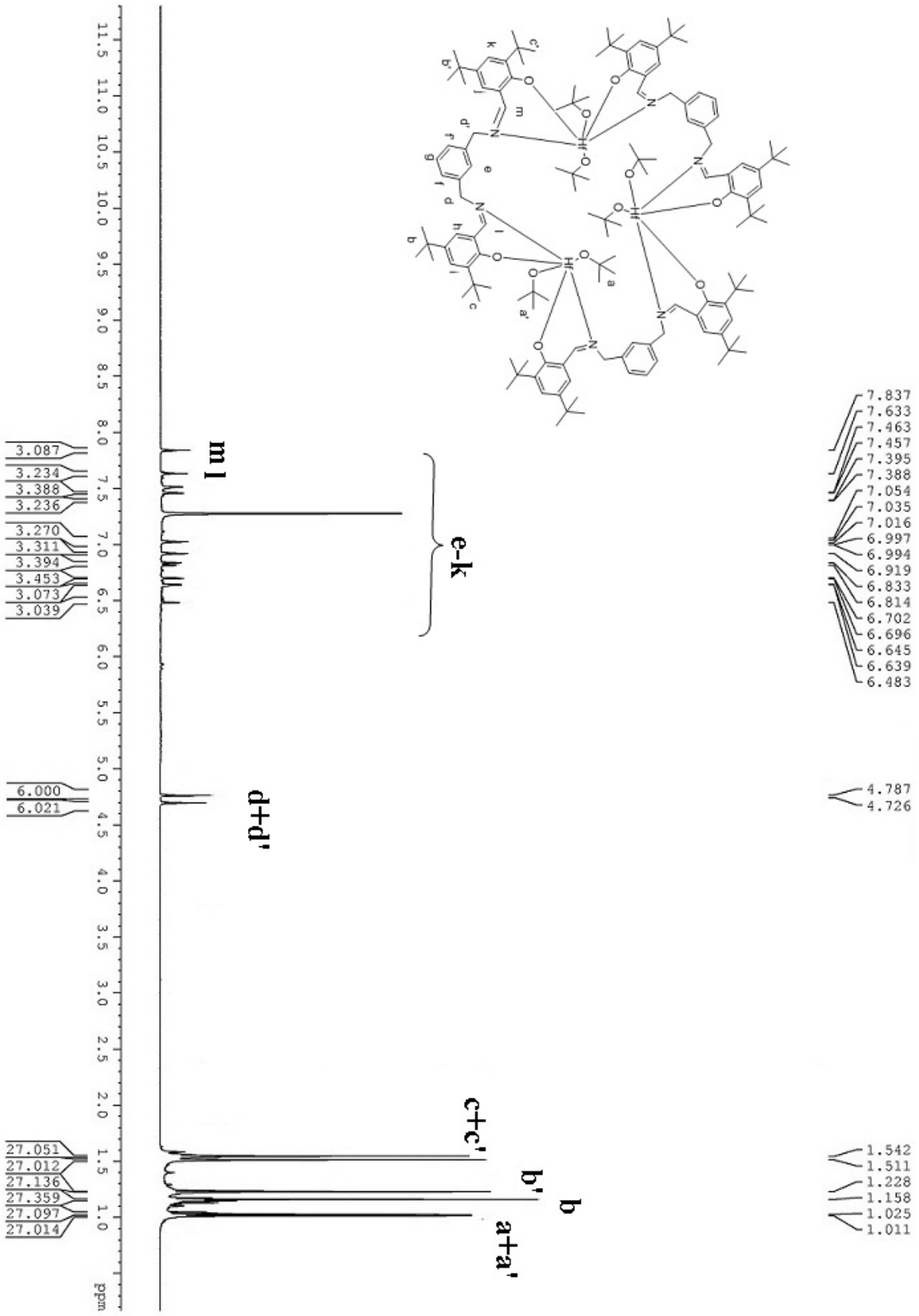

Figure S19. ^{1}H NMR (400 MHz, $CDCl_3$) of Compound **7**

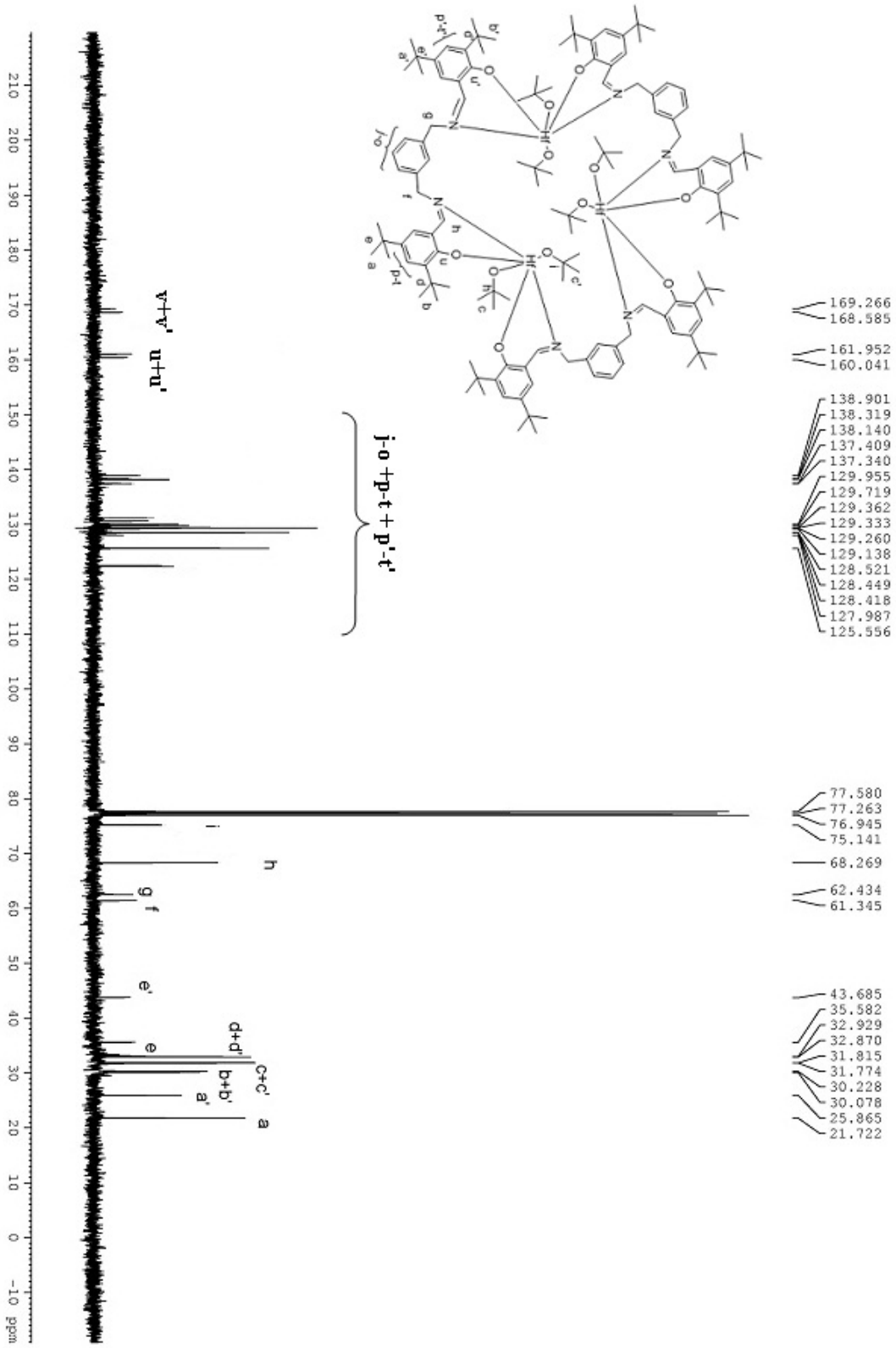

Figure S20. ^{13}C NMR (100 MHz, $CDCl_3$) of Compound **7**

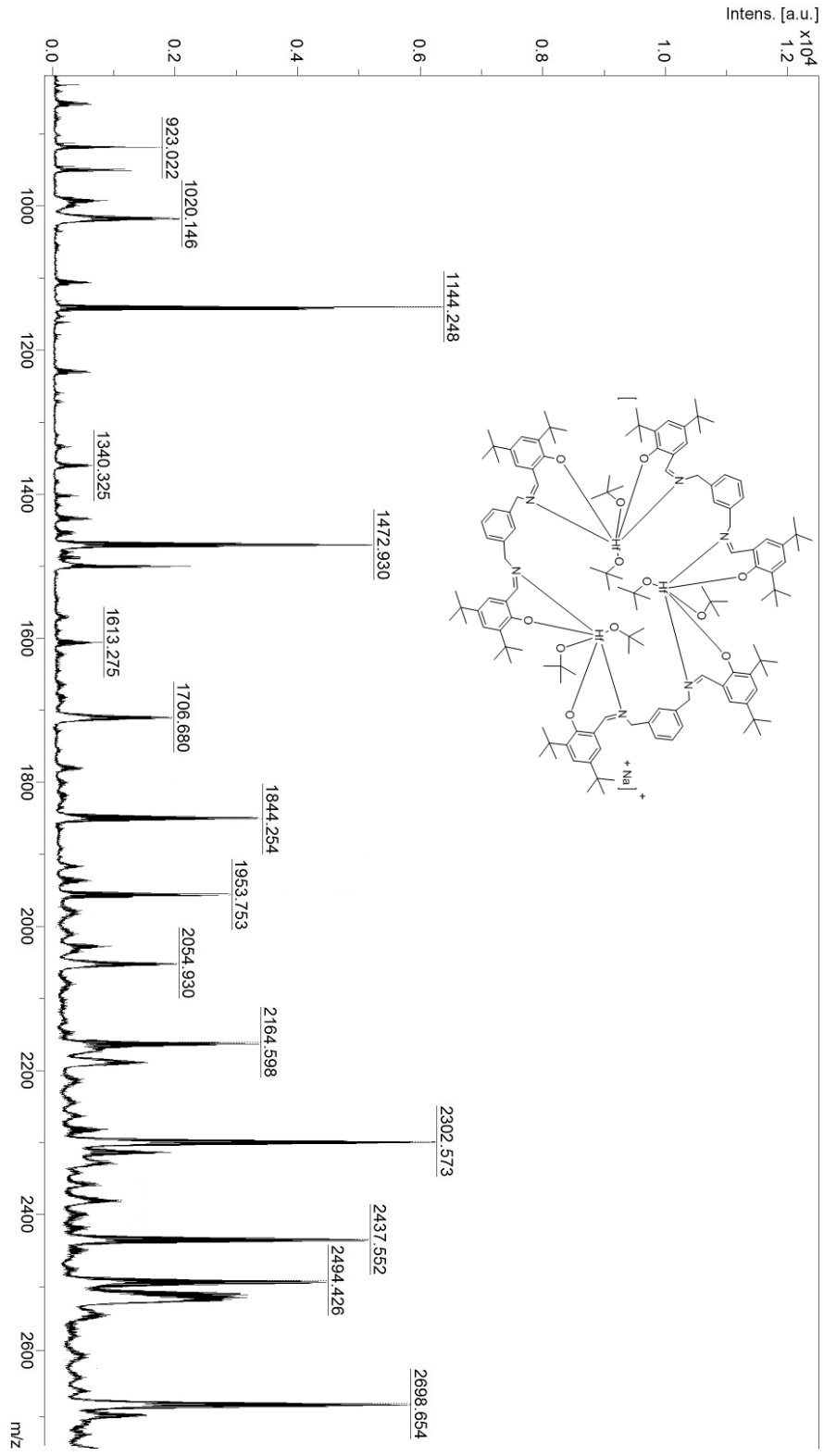

Figure S21.MALDI-TOF mass spectrum of Compound **7**

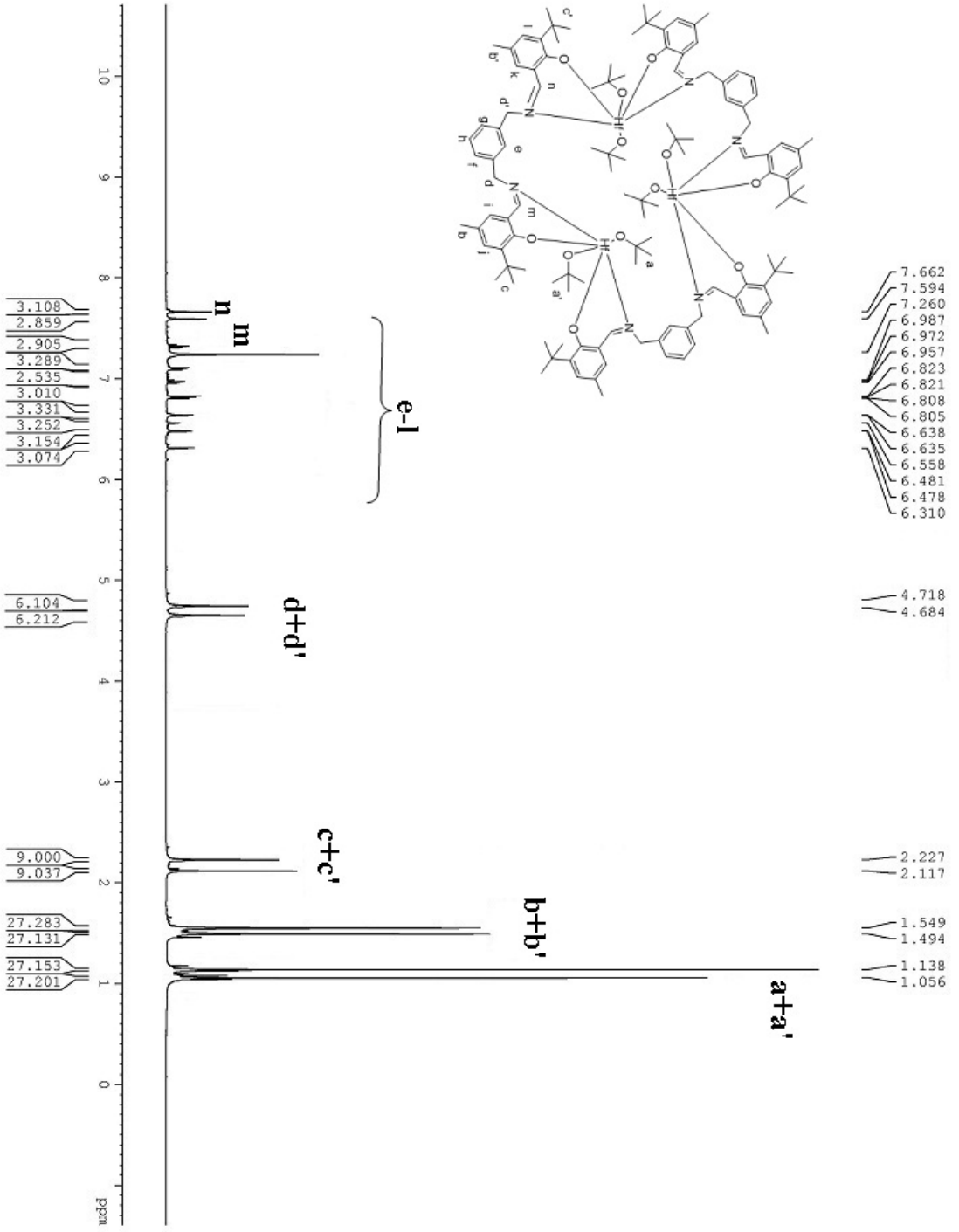

Figure S22. ^{1}H NMR (400 MHz, $CDCl_3$) of Compound **8**

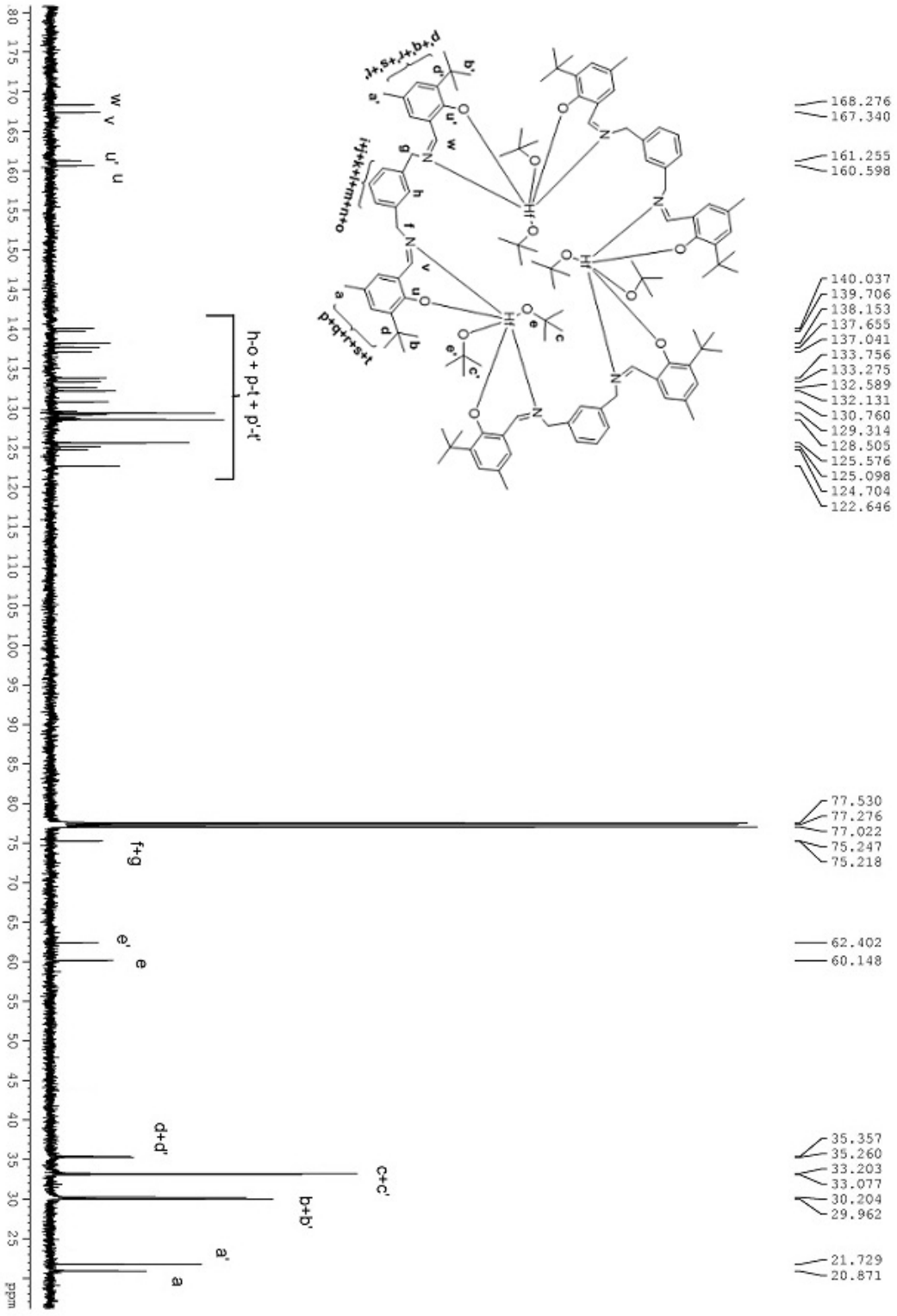

Figure S23. ^{13}C NMR (100 MHz, $CDCl_3$) of Compound **8**

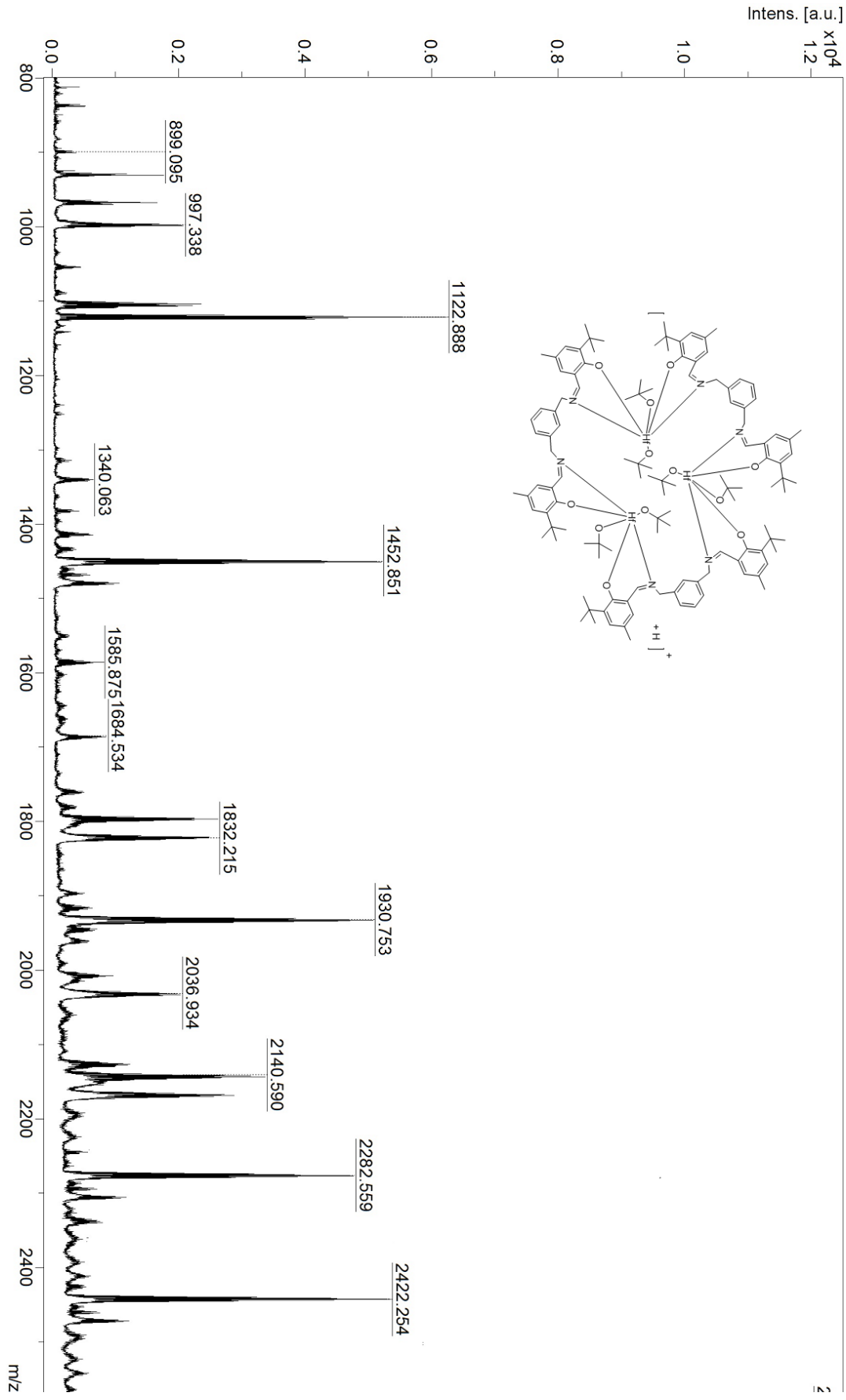

Figure S24.MALDI-TOF mass spectrum of Compound **8**

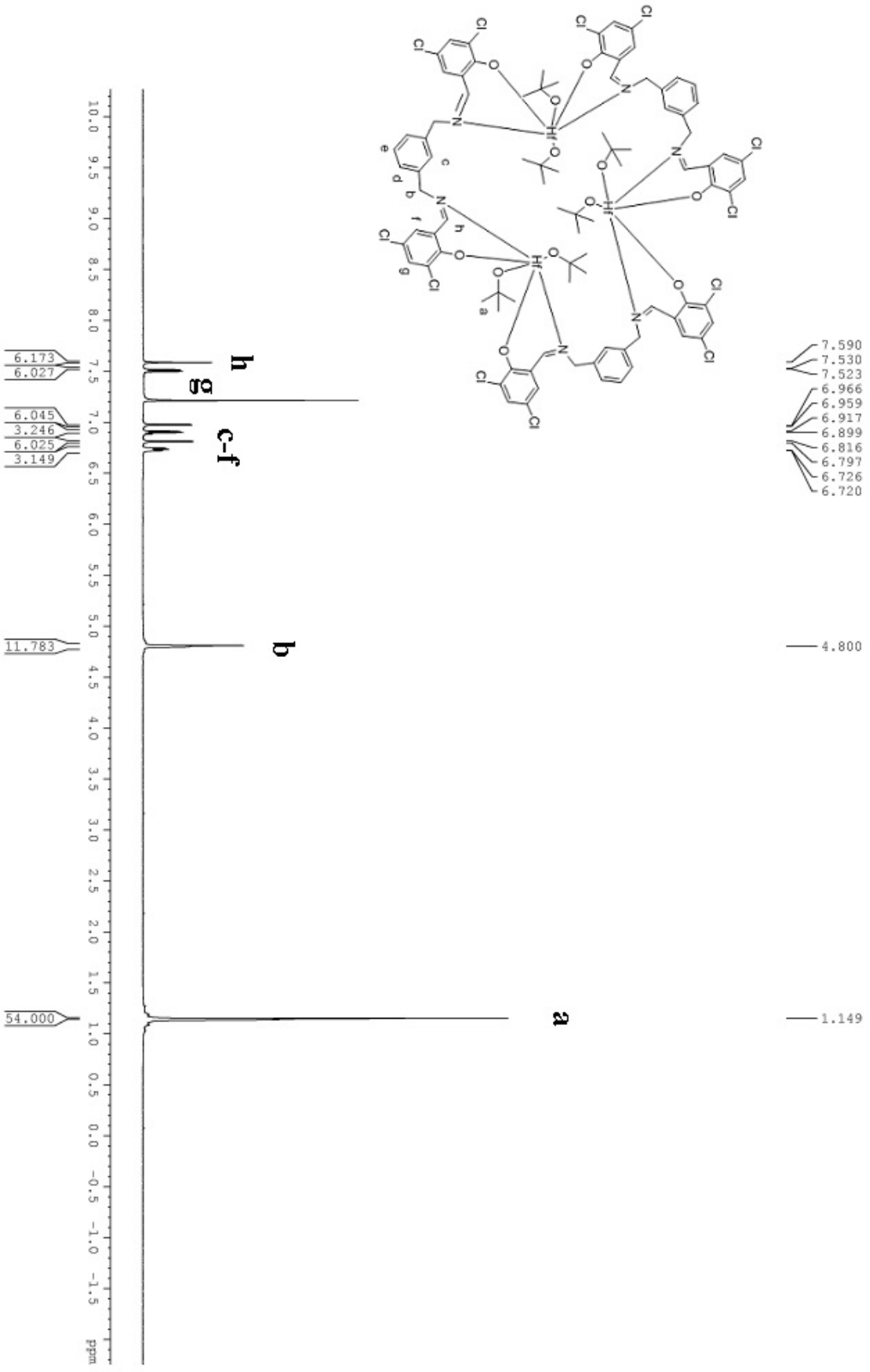

Figure S25.[1]H NMR (400 MHz, $CDCl_3$) of Compound **9**

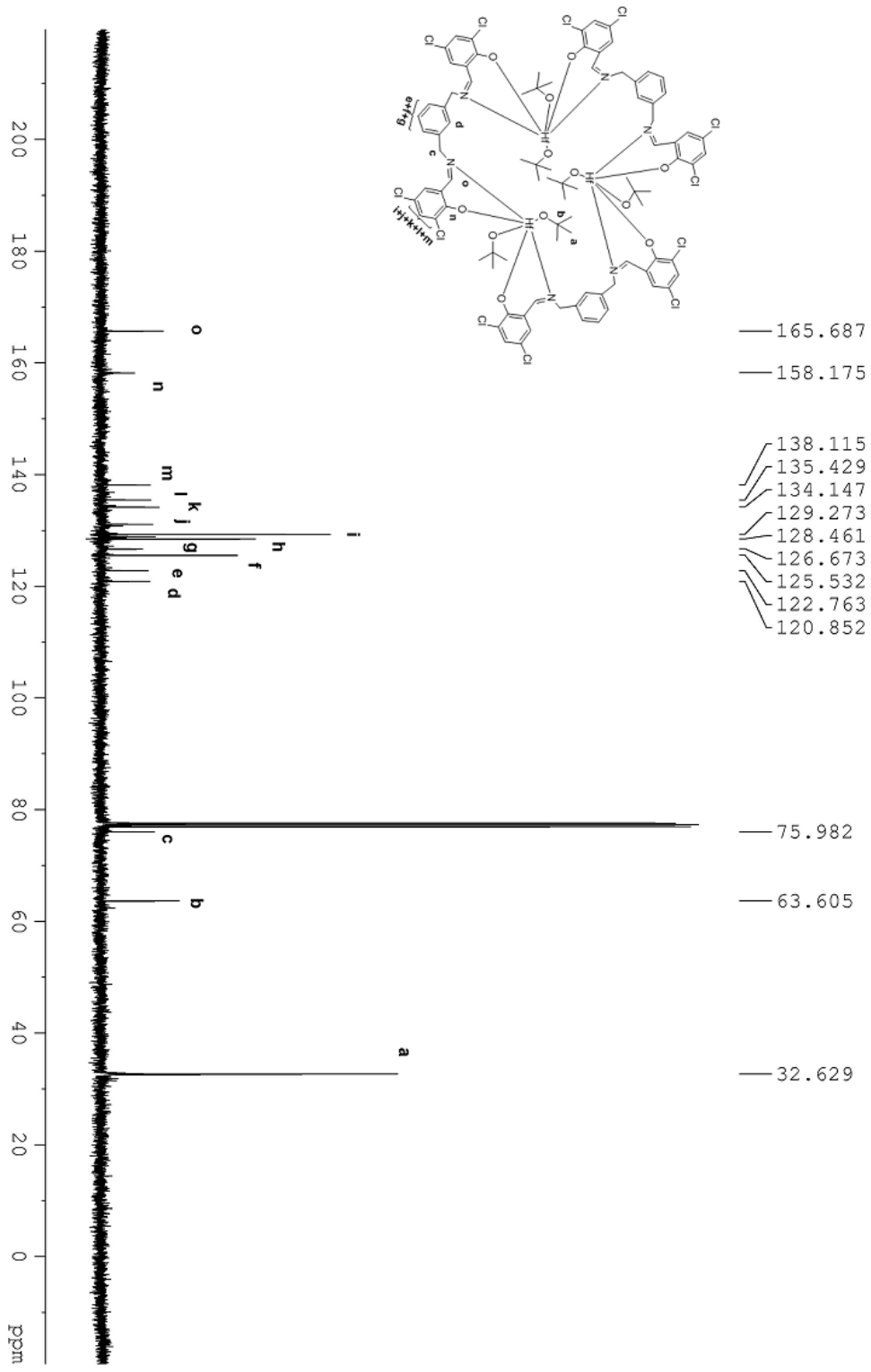

Figure S26. ^{13}C NMR (100 MHz, $CDCl_3$) of Compound **9**

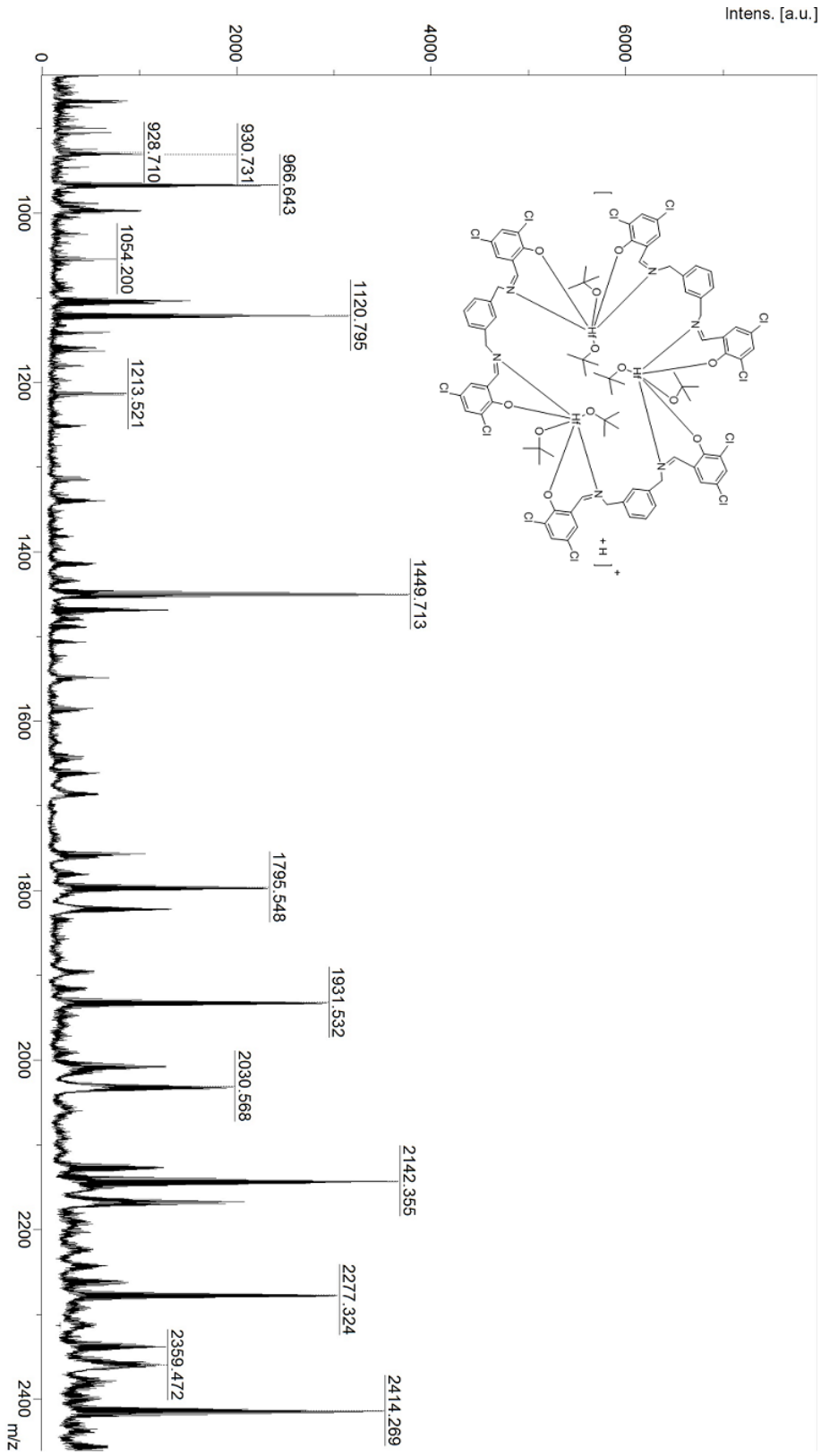

Figure S27.MALDI-TOF mass spectrum of Compound **9**

Polymerization details:

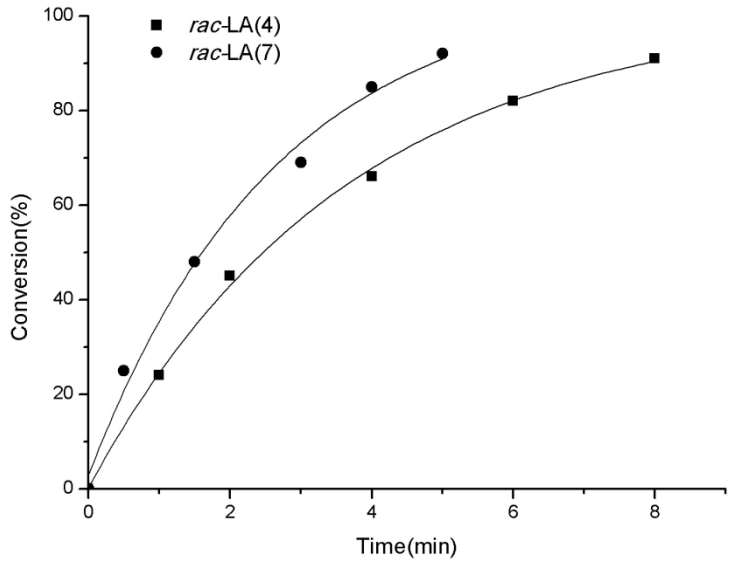

Figure S28. *rac*-LA conversion *vs* time plot using **4** and **7**: $[M]_o/[Cat]_o$= 200 at 140 °C

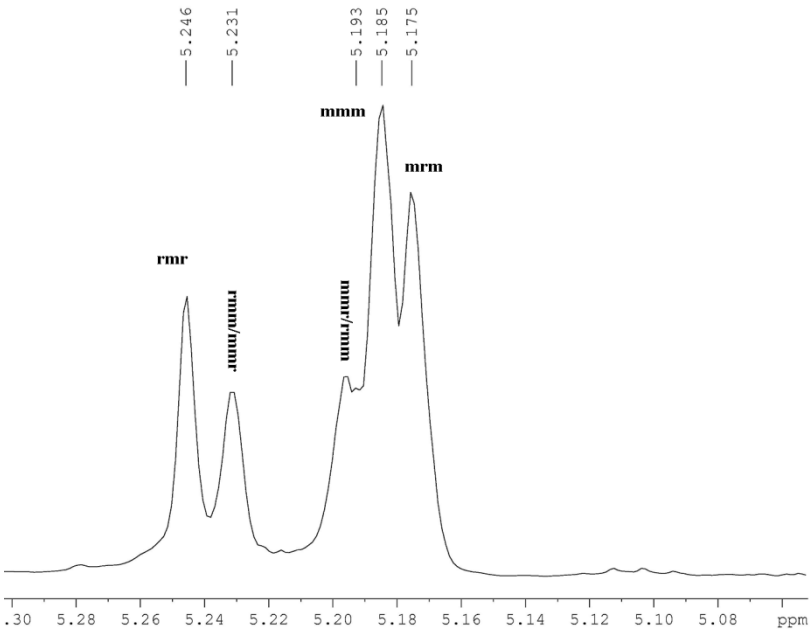

Figure S29. Homonuclear decoupled ^{1}H NMR (500 MHz, $CDCl_3$) spectrum of the methine region of PLA obtained using **1 (Table 2 Entry 1)**

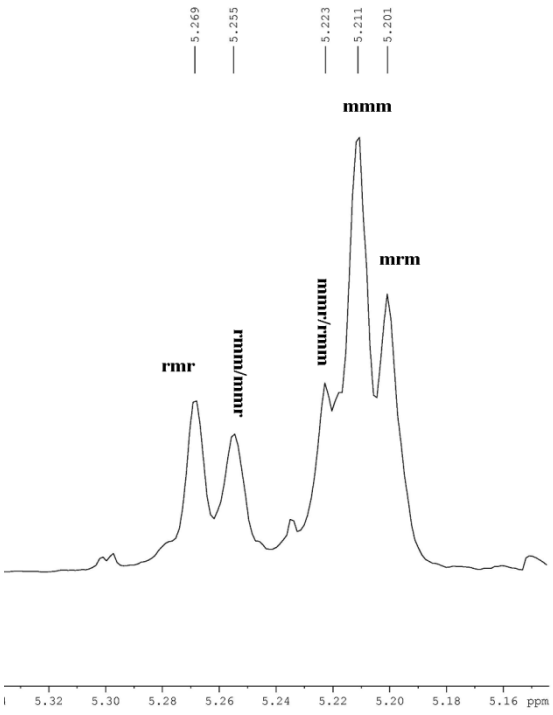

Figure S30. Homonuclear decoupled ^{1}H NMR (500 MHz, $CDCl_3$) spectrum of the methine region of PLA obtained using **5a (Table 2 Entry 6)**

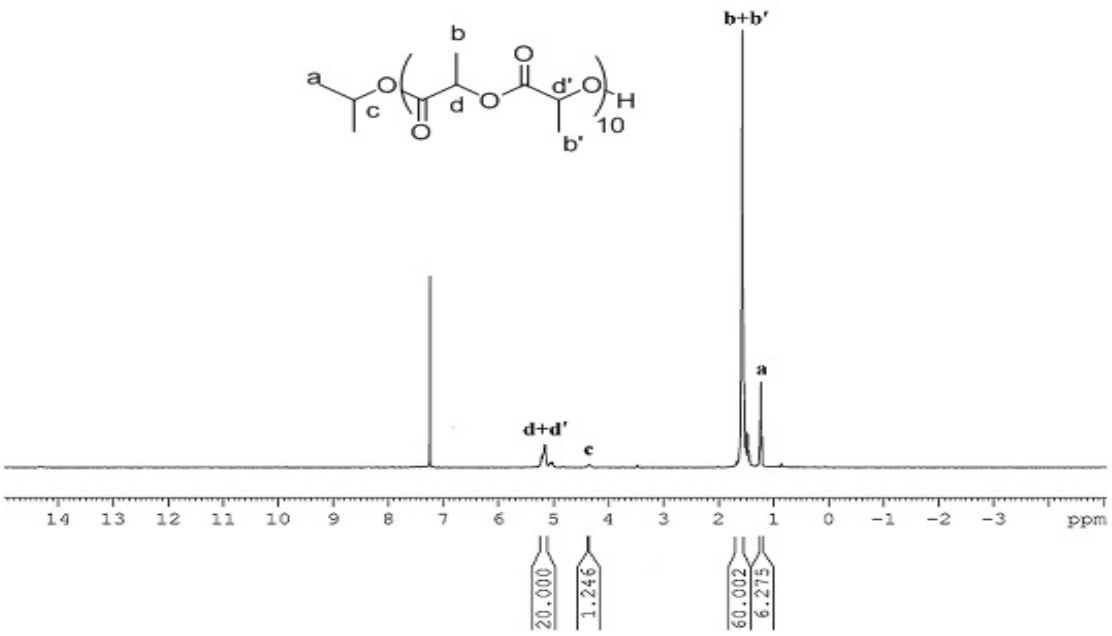

Figure S31. ^{1}H NMR spectrum (500 MHz, $CDCl_3$) of the crude product obtained from a reaction between *rac*-LA and **1** in 10:1 ratio at 140 °C

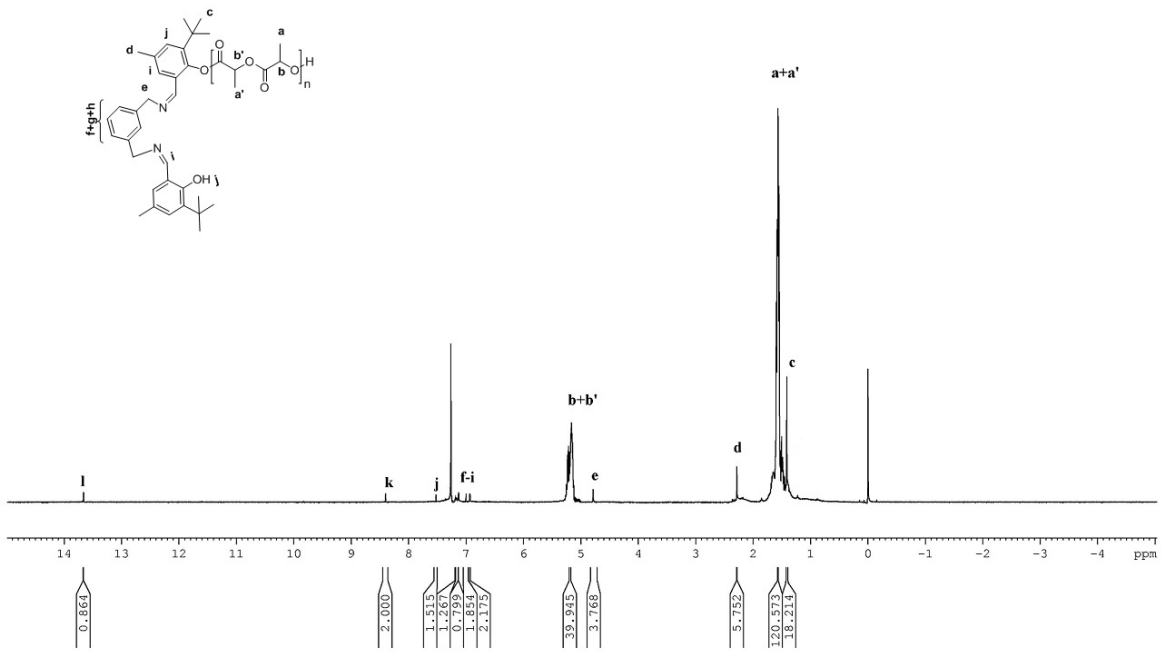

Figure S32. ^{1}H NMR spectrum (500 MHz, $CDCl_3$) of the crude product obtained from a reaction between *rac*-LA and **5a** in 20:1 ratio at 140 °C

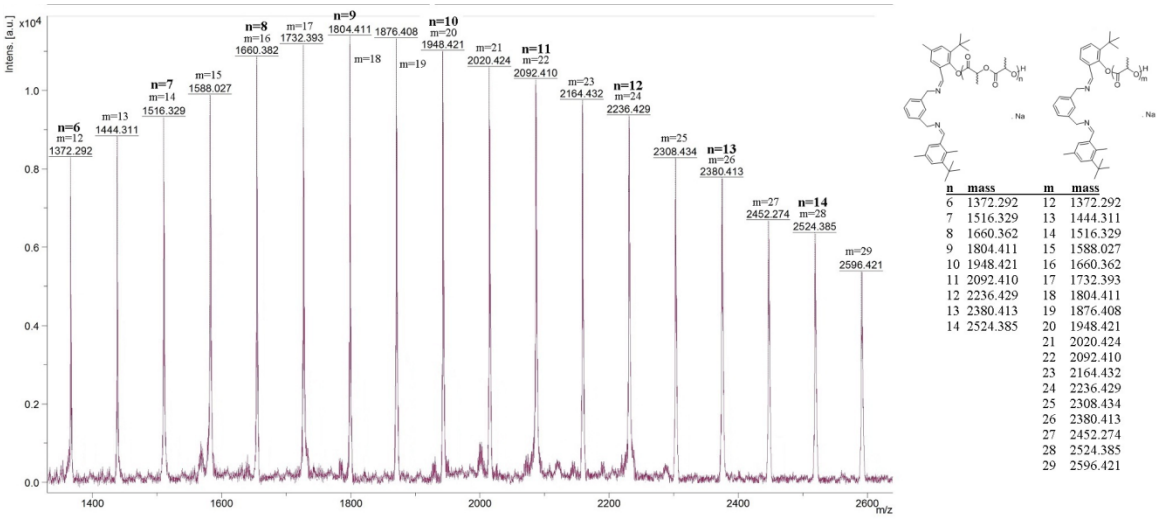

n	mass	m	mass
6	1372.292	12	1372.292
7	1516.329	13	1444.311
8	1660.362	14	1516.329
9	1804.411	15	1588.027
10	1948.421	16	1660.362
11	2092.410	17	1732.393
12	2236.429	18	1804.411
13	2380.413	19	1876.408
14	2524.385	20	1948.421
		21	2020.424
		22	2092.410
		23	2164.432
		24	2236.429
		25	2308.434
		26	2380.413
		27	2452.274
		28	2524.385
		29	2596.421

Figure S33.MALDI-TOF spectrum of the crude product obtained from a reaction between *rac*-LA and **5a** in 20:1 ratio at 140 °C

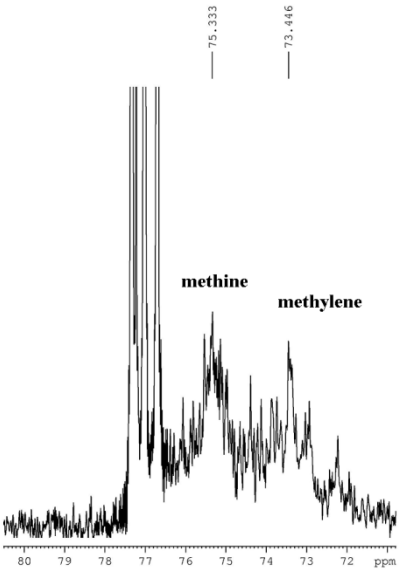

Figure S34. C^{13} {^{1}H} NMR spectrum (400 MHz, $CDCl_3$) showing the methine and methylene carbons for the regioirregular polymer obtained from a reaction between *rac*-PO and **1** in 1000:1 ratio at 30 °C

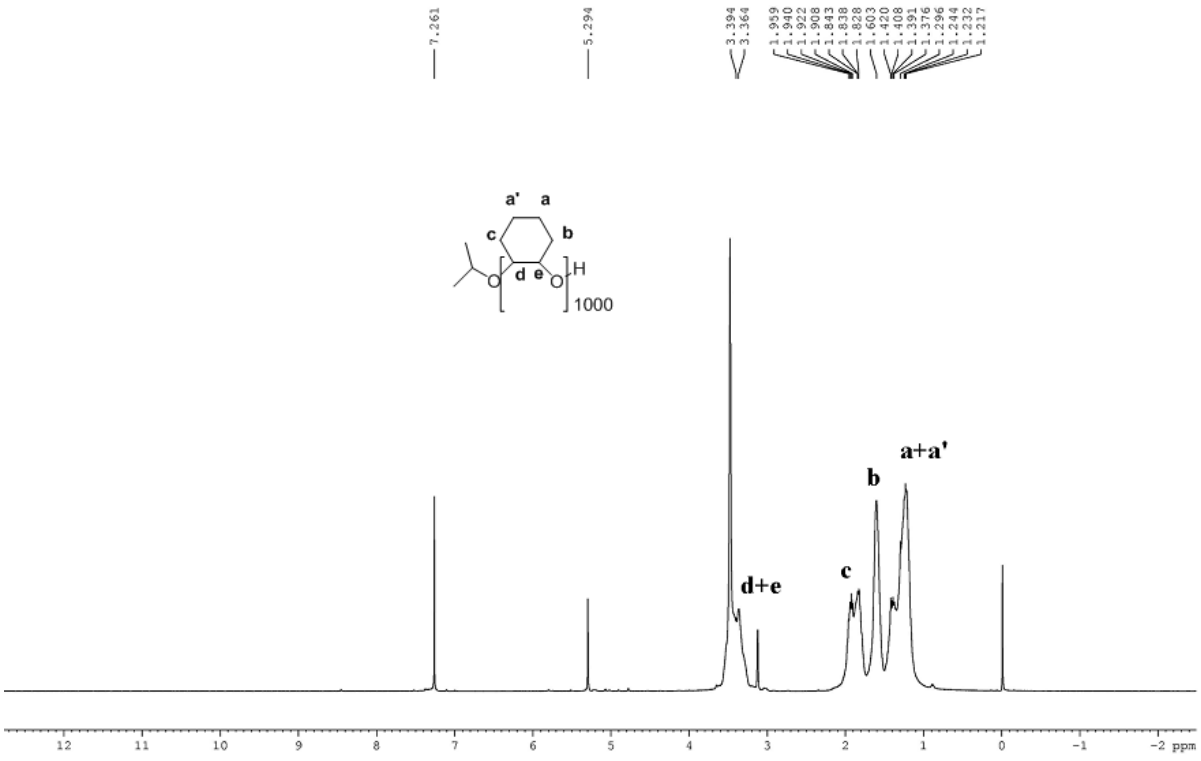

Figure S35.^{1}H NMR spectrum (500 MHz, $CDCl_3$) of the crude product obtained from a reaction between CHO and **1** in 1000:1 ratio at 100 °C

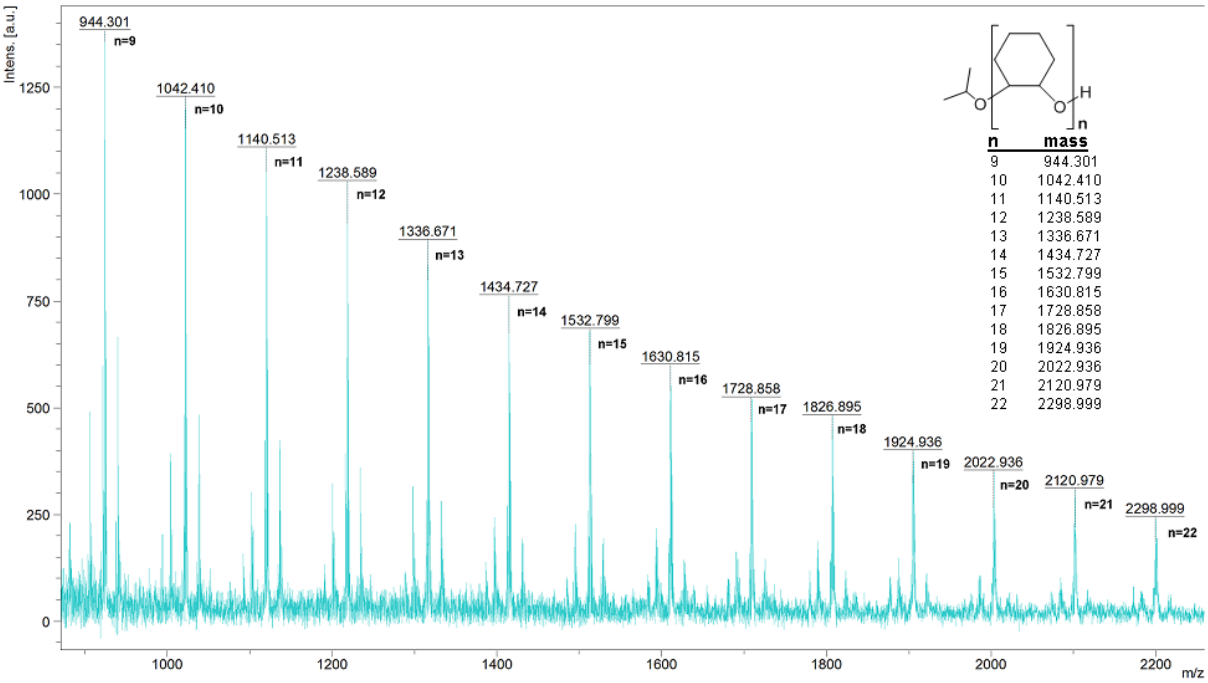

Figure S36.MALDI-TOF spectrum of the crude product obtained from a reaction between CHO and **1** in 1000:1 ratio at 100 °C

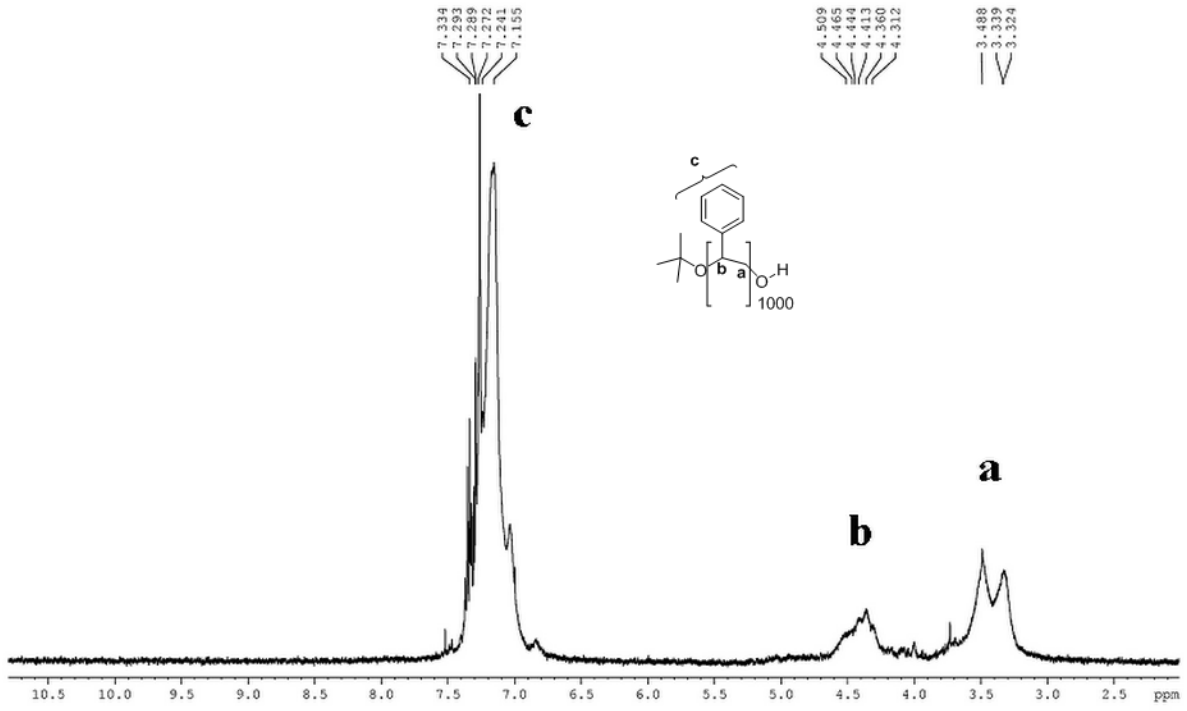

Figure S37.^{1}H NMR spectrum (500 MHz, $CDCl_3$) of the crude product obtained from a reaction between SO and **7** in 1000:1 ratio at 130 °C

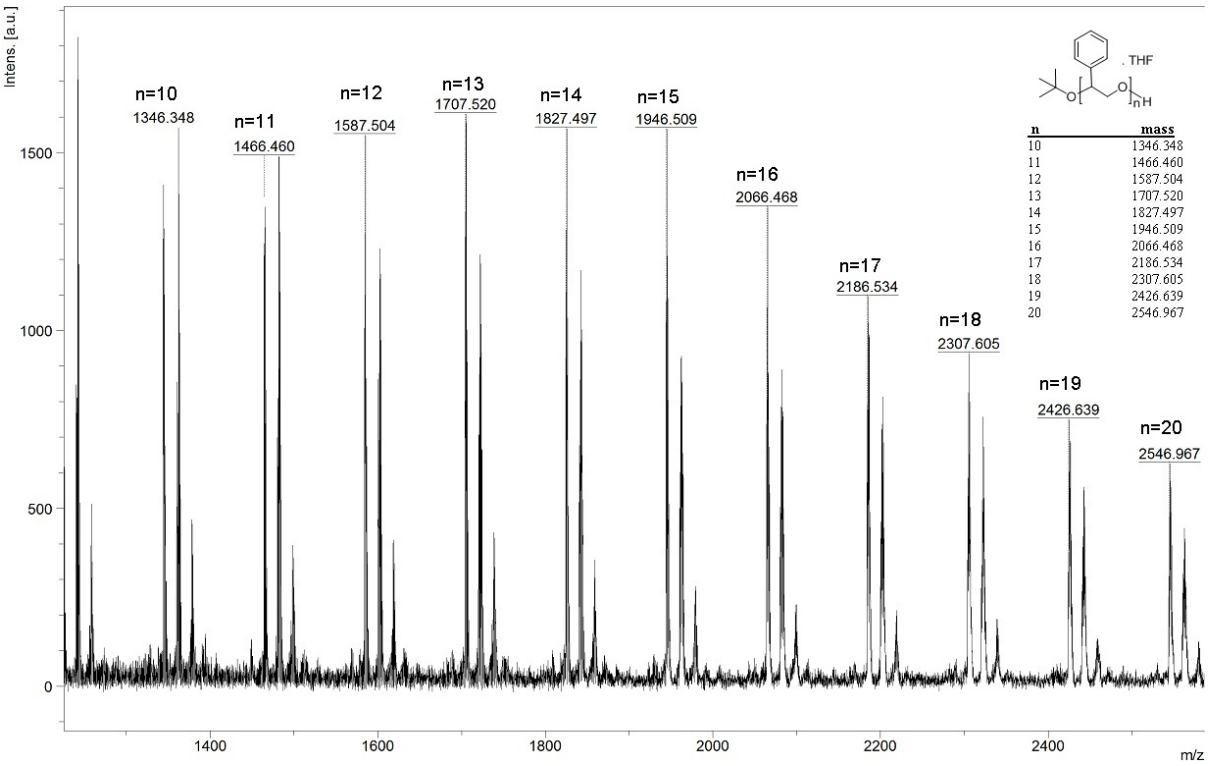

Figure S38.MALDI-TOF spectrum of the crude product obtained from a reaction between SO and **7** in 1000:1 ratio at 130 °C

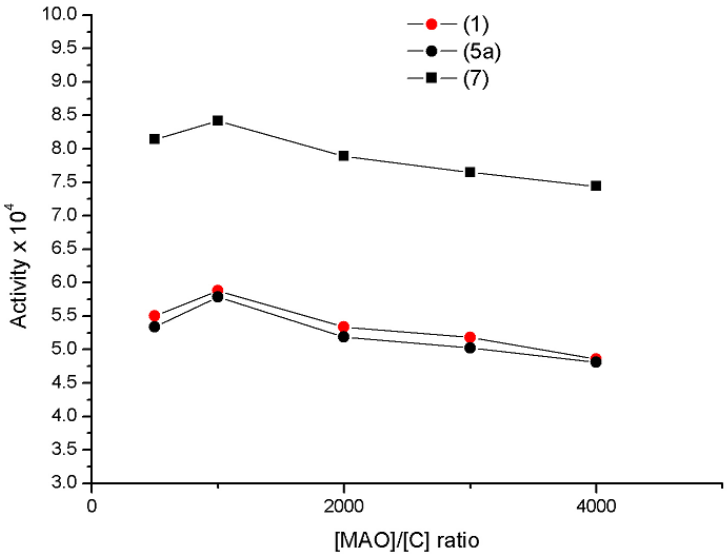

Figure S39. Plot of activity *vs* [MAO]/[C] ratio for **1**, **5a** and **7** for ethylene polymerization

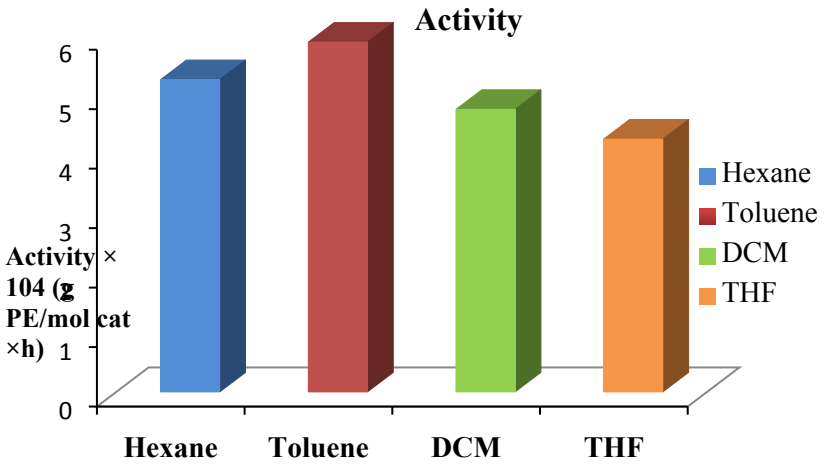

Figure S40. Activity of **1** in different solvent in ethylene polymerization

Computational details:

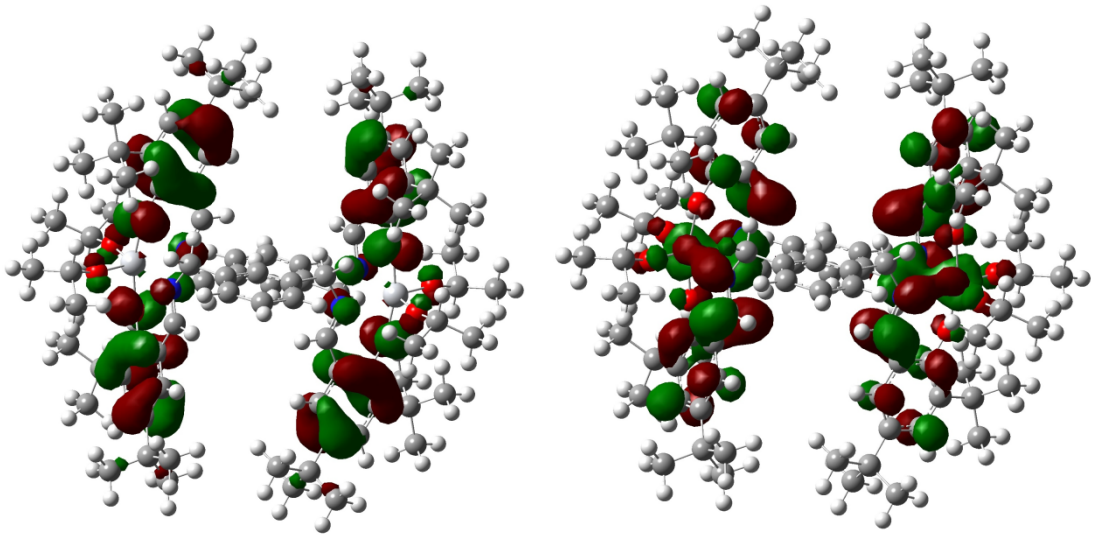

1

HOMO = -5.36 eV LUMO = -1.61 eV

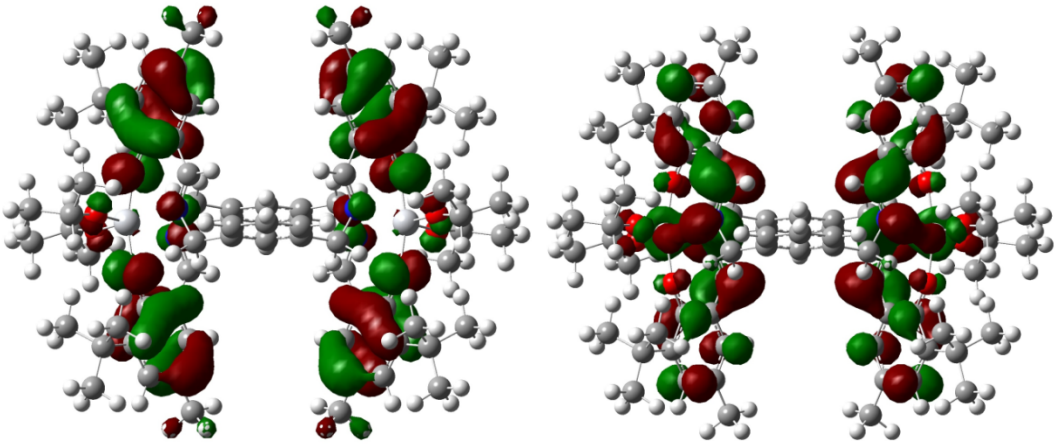

2

HOMO = -5.36 eV LUMO = -1.63 eV

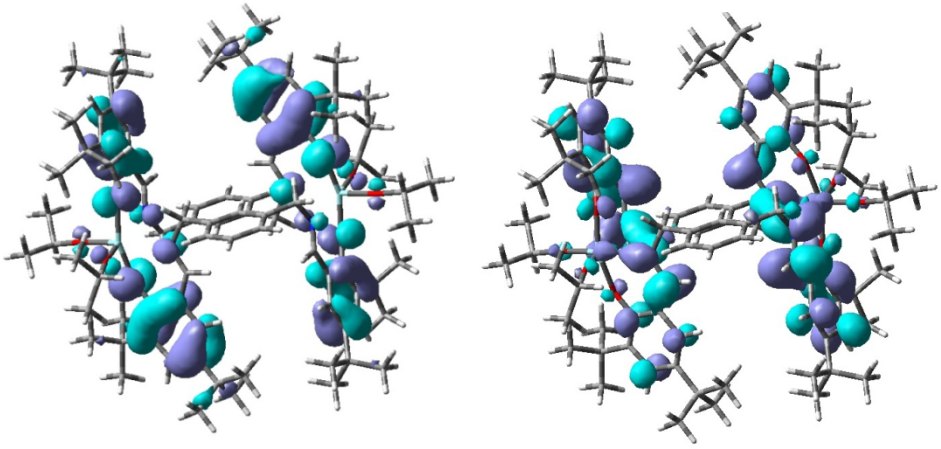

4

HOMO = -5.47 eV LUMO = -1.74 eV

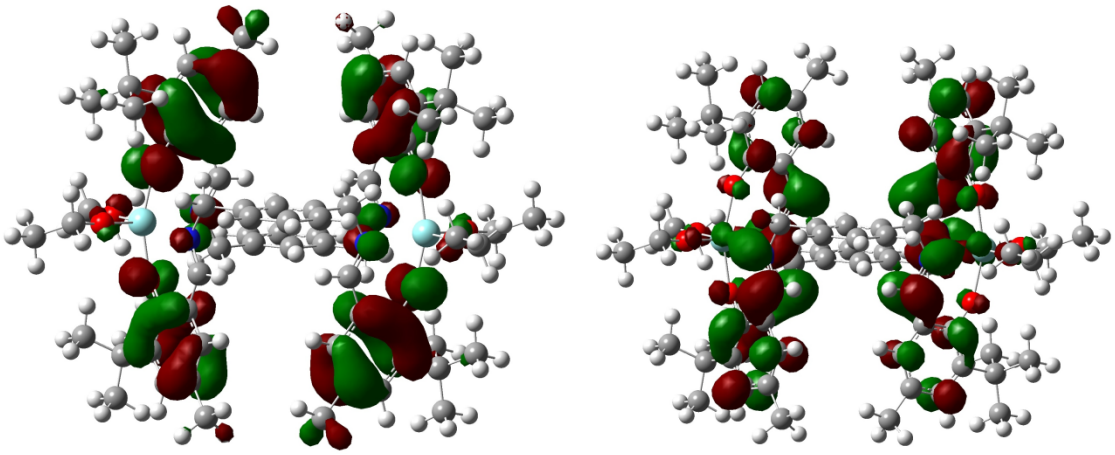

5a

HOMO = -5.47 eV LUMO = -1.74 eV

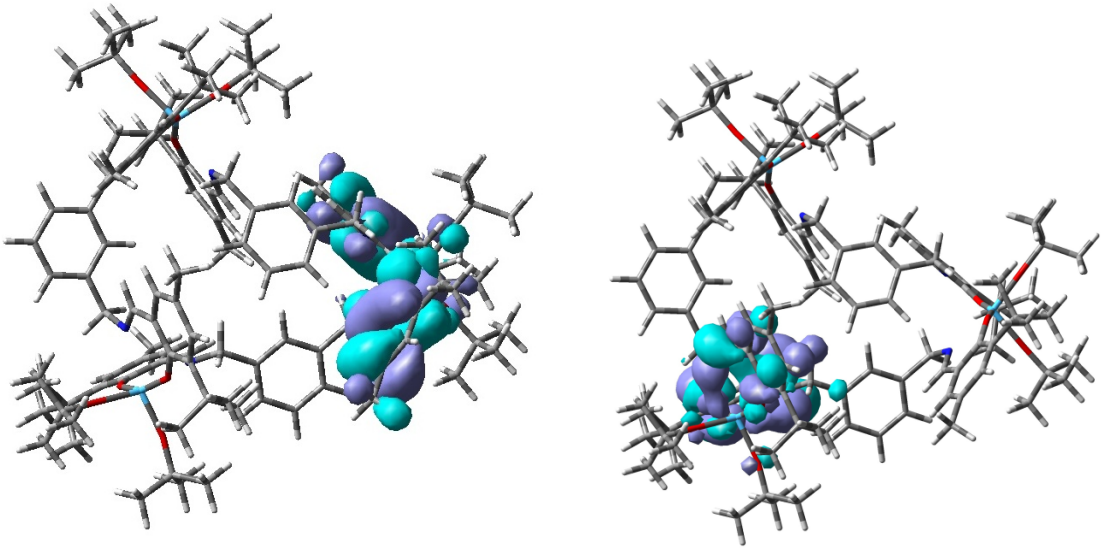

8

HOMO = -5.50 eV LUMO = -1.85 eV

Figure S41. Frontier molecular orbital diagrams of complexes **1**, **2**, **4**, **5a** and **8**

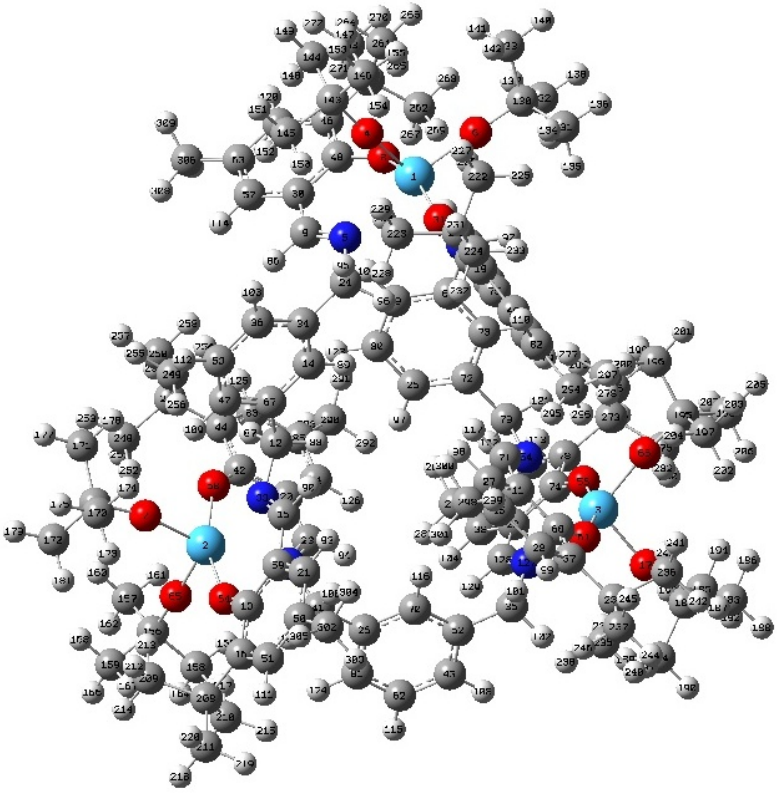

Figure S42. Optimized geometry of **8** with atom numbering scheme

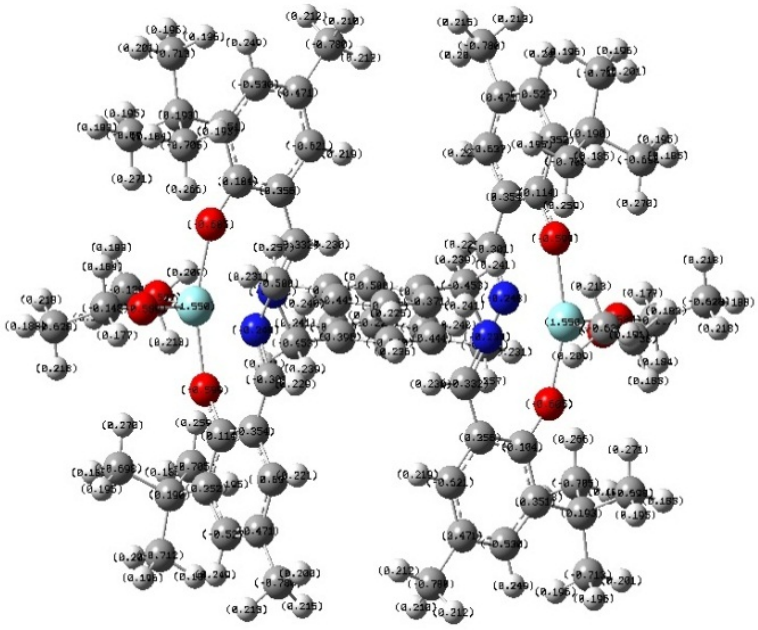

Figure S43. Mulliken partial charges of complex **5a**

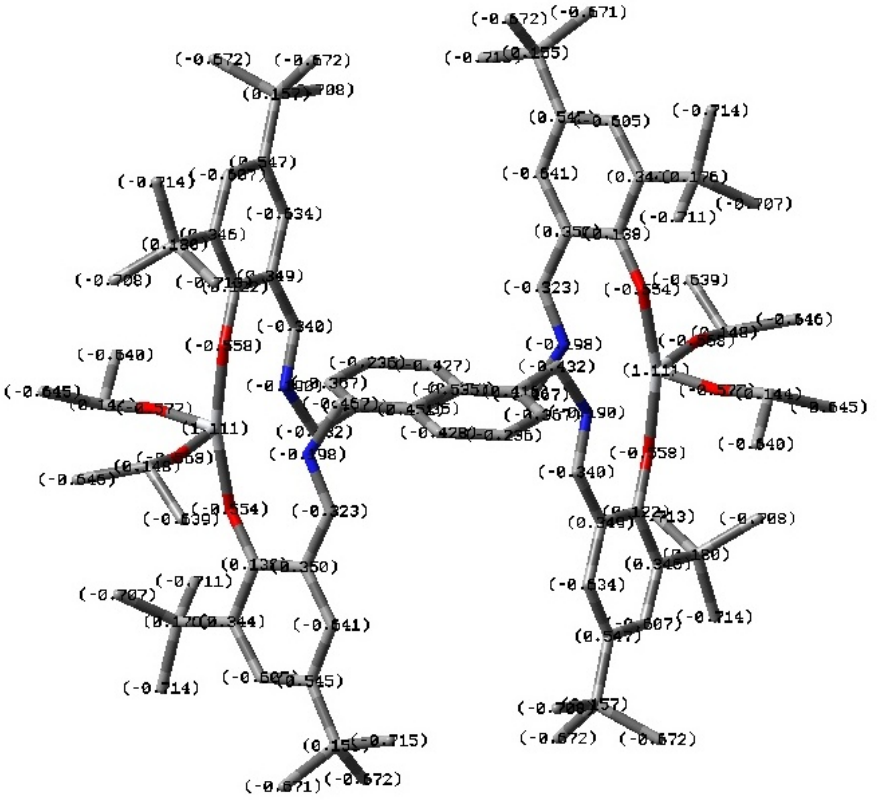

1

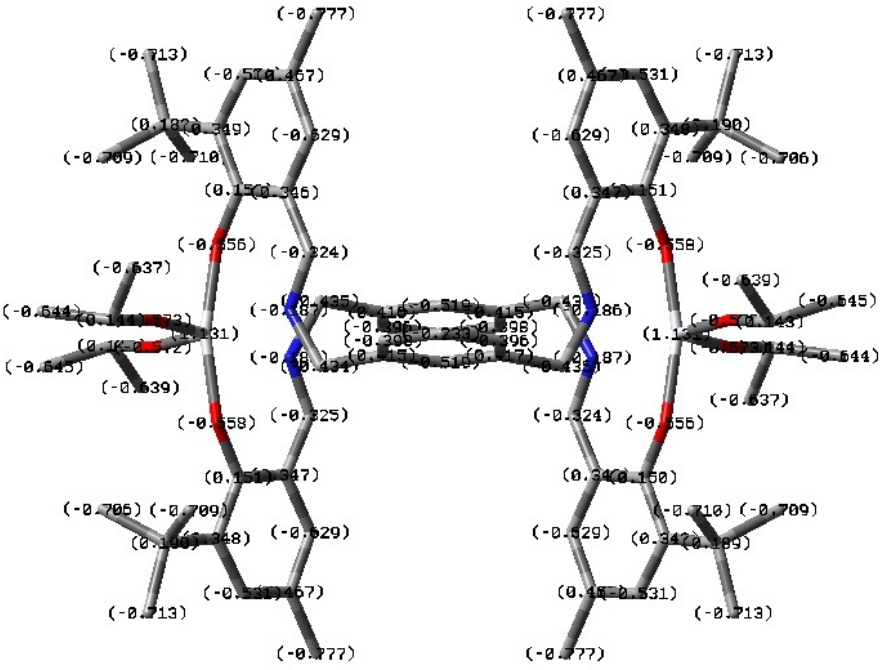

2

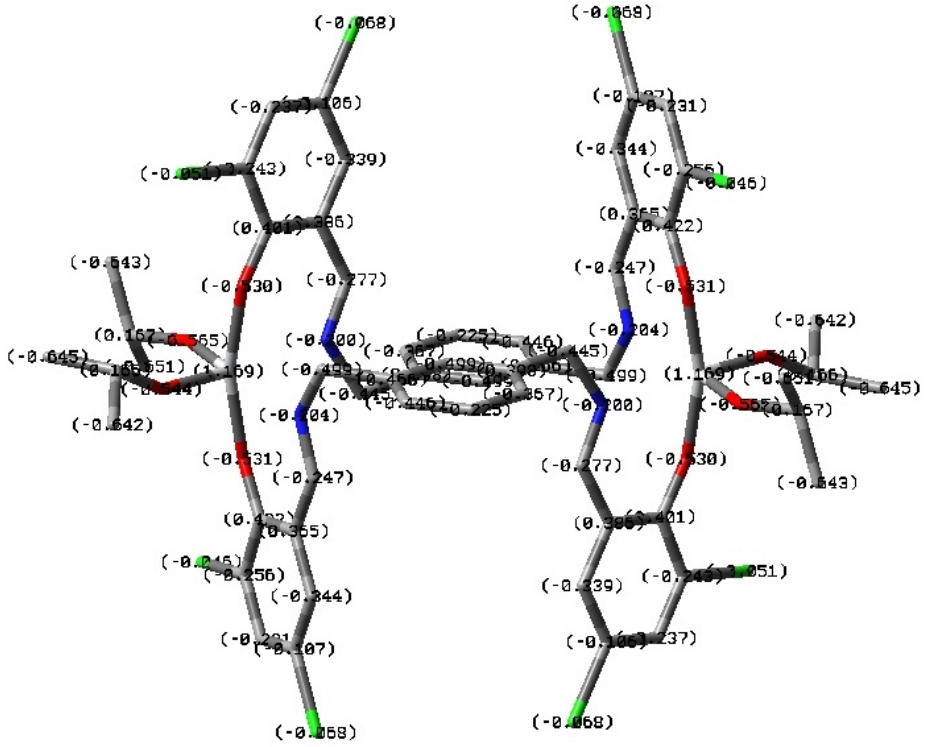

3

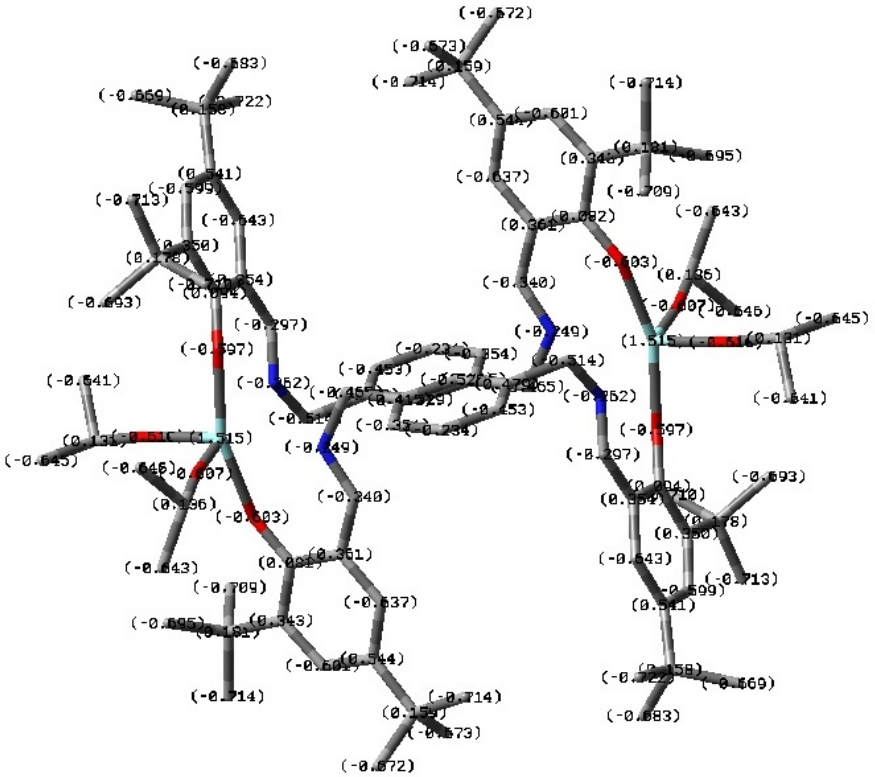

4

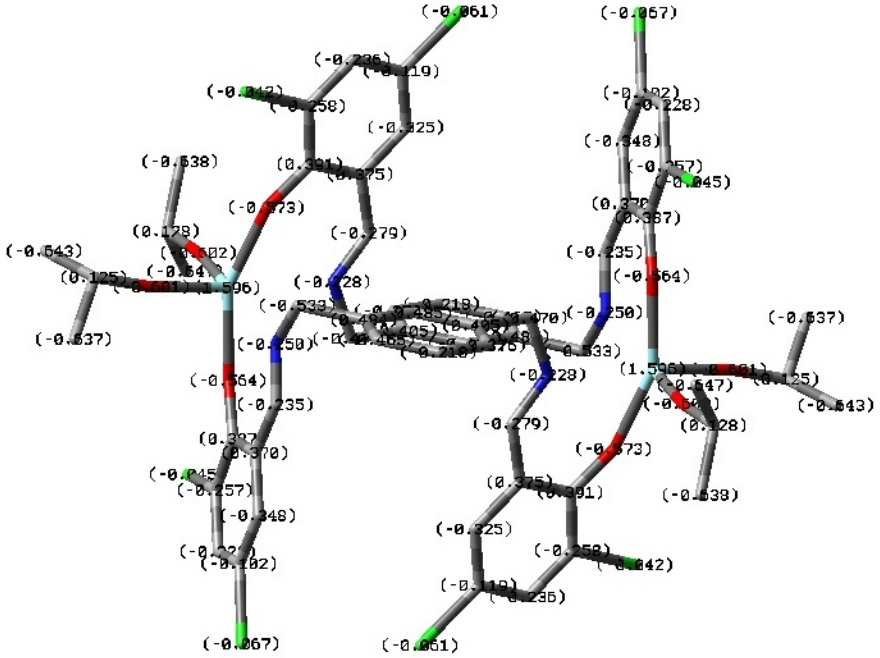

6

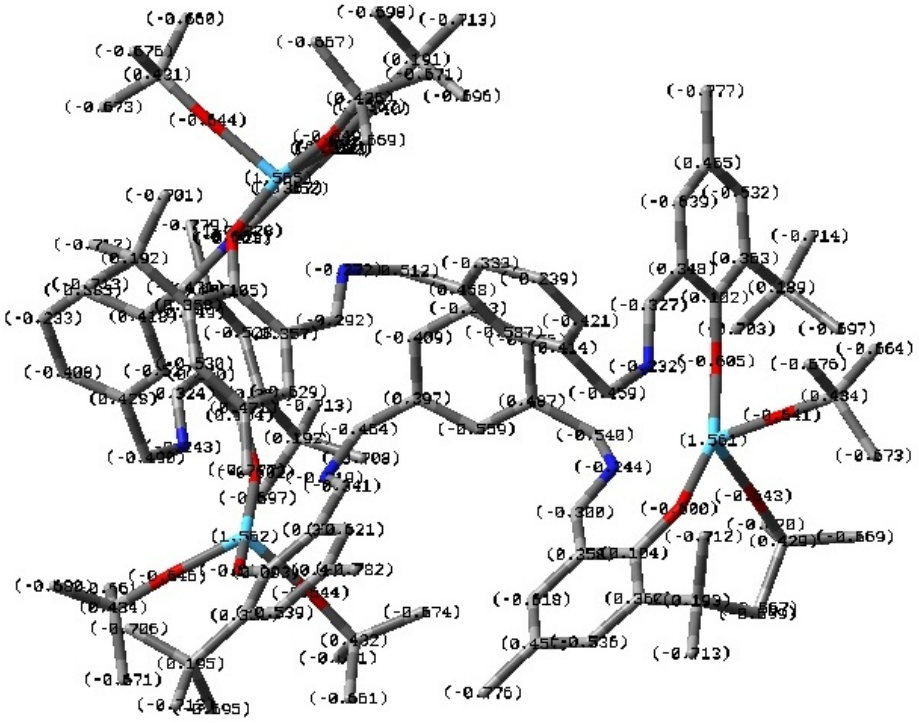

8

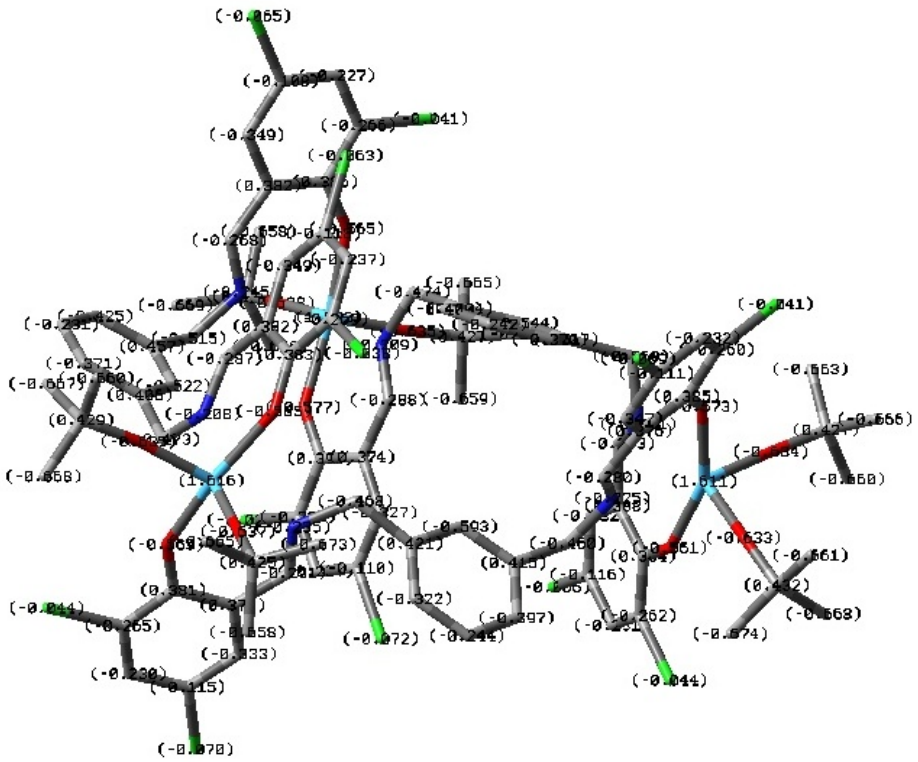

9

Figure S44. Mulliken partial charges of complexes **1**, **2**, **3**, **4**, **6**, **8** and **9**

Table S1. Selected X-ray and calculated bond lengths and bond angles of **1, 5a** and **7**

S. No.	Compound	Bond Length (Å)			Bond Angle (°)		
		Entry	X-ray	Calculated	Entry	X-ray	Calculated
1.	**1**	O1-Ti1	1.89(7)	1.92	O1-Ti1-O3	94.4(3)	95.8
2.		O3-Ti1	1.75(5)	1.75	O1-Ti1-O2	165.2(3)	165.2
3.		O2-Ti1	1.89(7)	1.89	O3-Ti1-O4	104.4(3)	104.7
4.		N2-Ti1	2.24(7)	2.29	O1-Ti1-N2	87.6(3)	88.5
5.		N1-Ti1	2.27(7)	2.28	N2-Ti1-N1	78.1(3)	79.6
6.	**5a**	O1-Zr1	2.03(3)	2.08	O1-Zr1-O2	96.8(2)	97.4
7.		O2-Zr1	1.93(5)	1.96	O1-Zr1-N2	76.4(1)	76.0
8.		O4-Zr1	2.03(3)	2.08	O1-Zr1-O3	106.2(2)	104.3
9.		N2-Zr1	2.41(3)	2.42	N2-Zr1-N1	76.2(1)	79.1
10.		N1-Zr1	2.41(4)	2.43	O1-Zr1-O4	161.4(1)	160.7

11.		O2-C36	1.39(1)	1.42	O2-C36-C37	115(1)	111.7
12.		O3-C34	1.41(9)	1.42	O3-C34-C35	112.2(8)	111.3
13.	**7**	O1-Hf1	2.04(7)	2.05	O1-Hf1-O4	96.8(3)	96.1
14.		O4-Hf1	1.91(6)	1.94	O1-Hf1-O2	158.4(3)	159.6
15.		O3-Hf1	1.91(8)	1.93	O3-Hf1-O4	102.7(3)	103.5
16.		N1-Hf1	2.36(8)	2.39	N1-Hf1-N2	81.1(3)	81.1
17.		O12-Hf2	2.02(8)	2.05	O9-Hf2-O12	156.8(3)	158.4
18.		O10-Hf2	1.92(8)	1.94	O9-Hf2-O11	95.9(3)	95.2
19.		N5-Hf2	2.41(9)	2.40	N5-Hf2-N6	80.5(3)	79.5
20.		N6-Hf2	2.39(8)	2.40	O10-Hf2-O11	102.7(3)	103.1

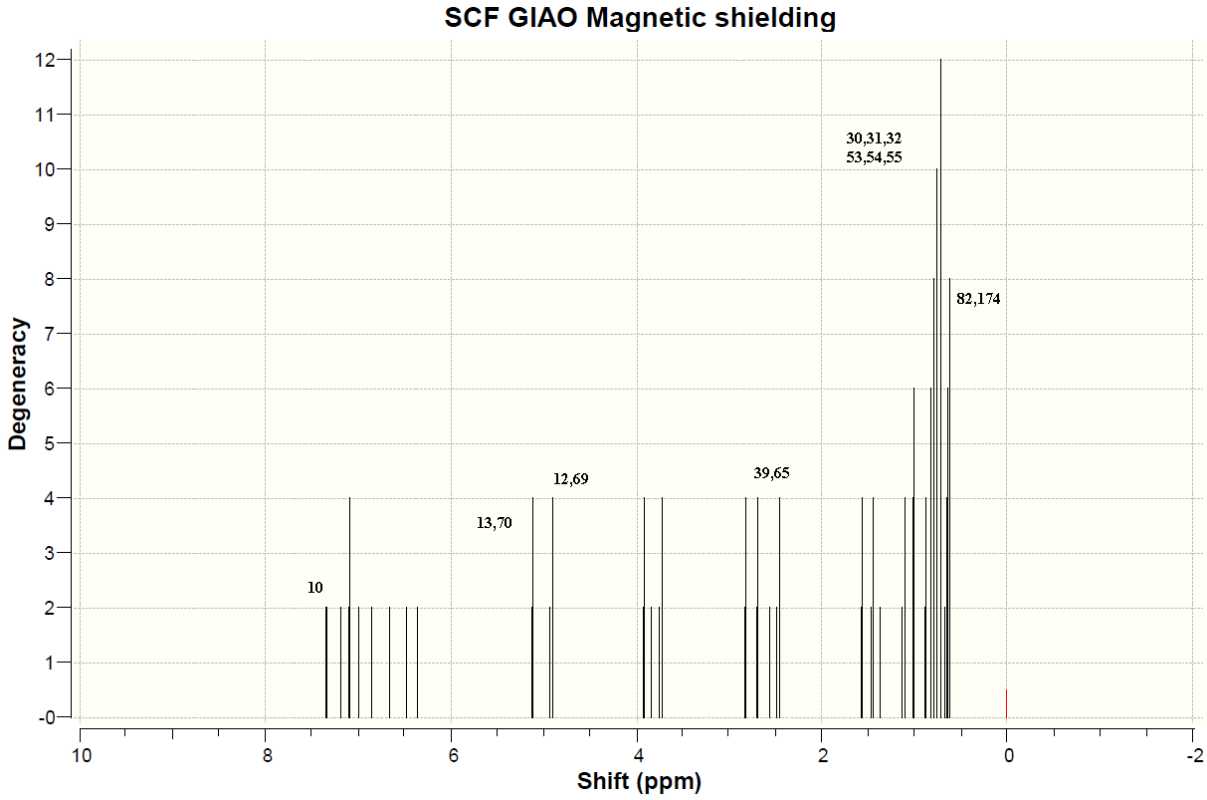

Figure S45. SCF GIAO magnetic shielding of ^{1}H atoms in **5a**

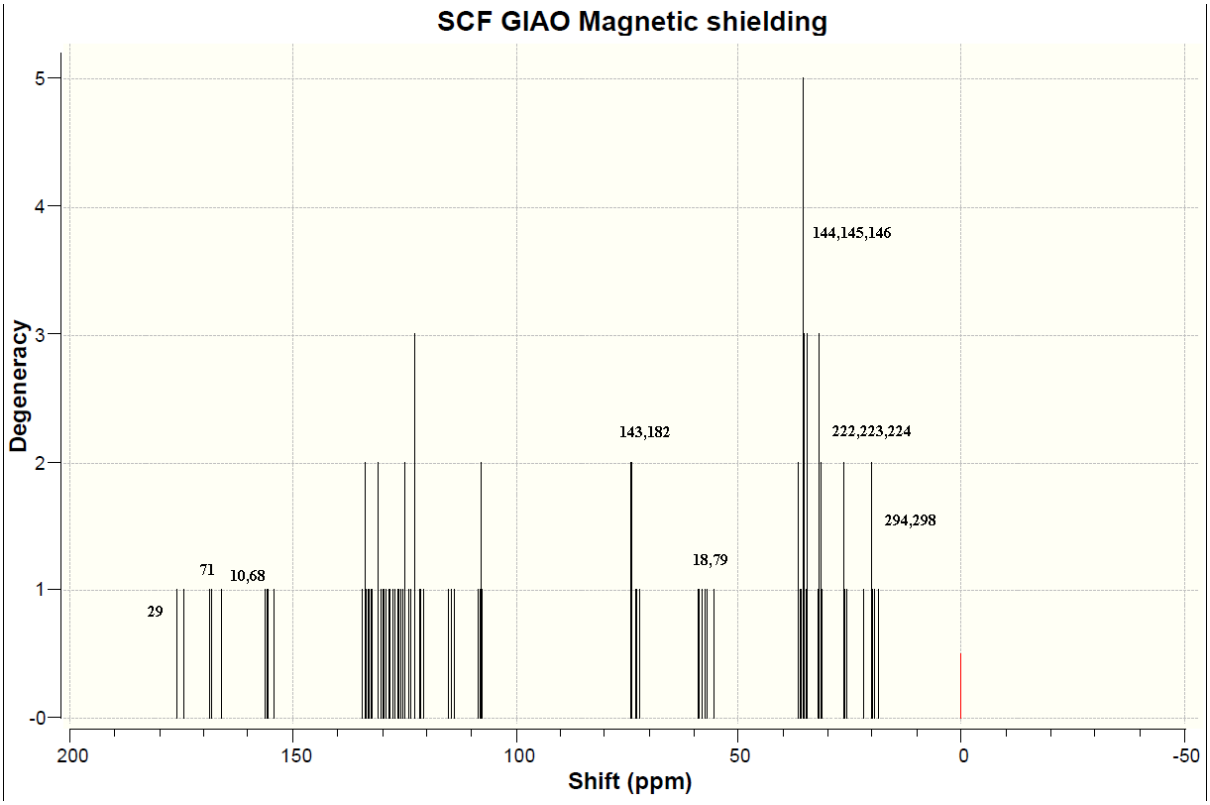

Figure S46. SCF GIAO magnetic shielding of ^{13}C atoms in **8**

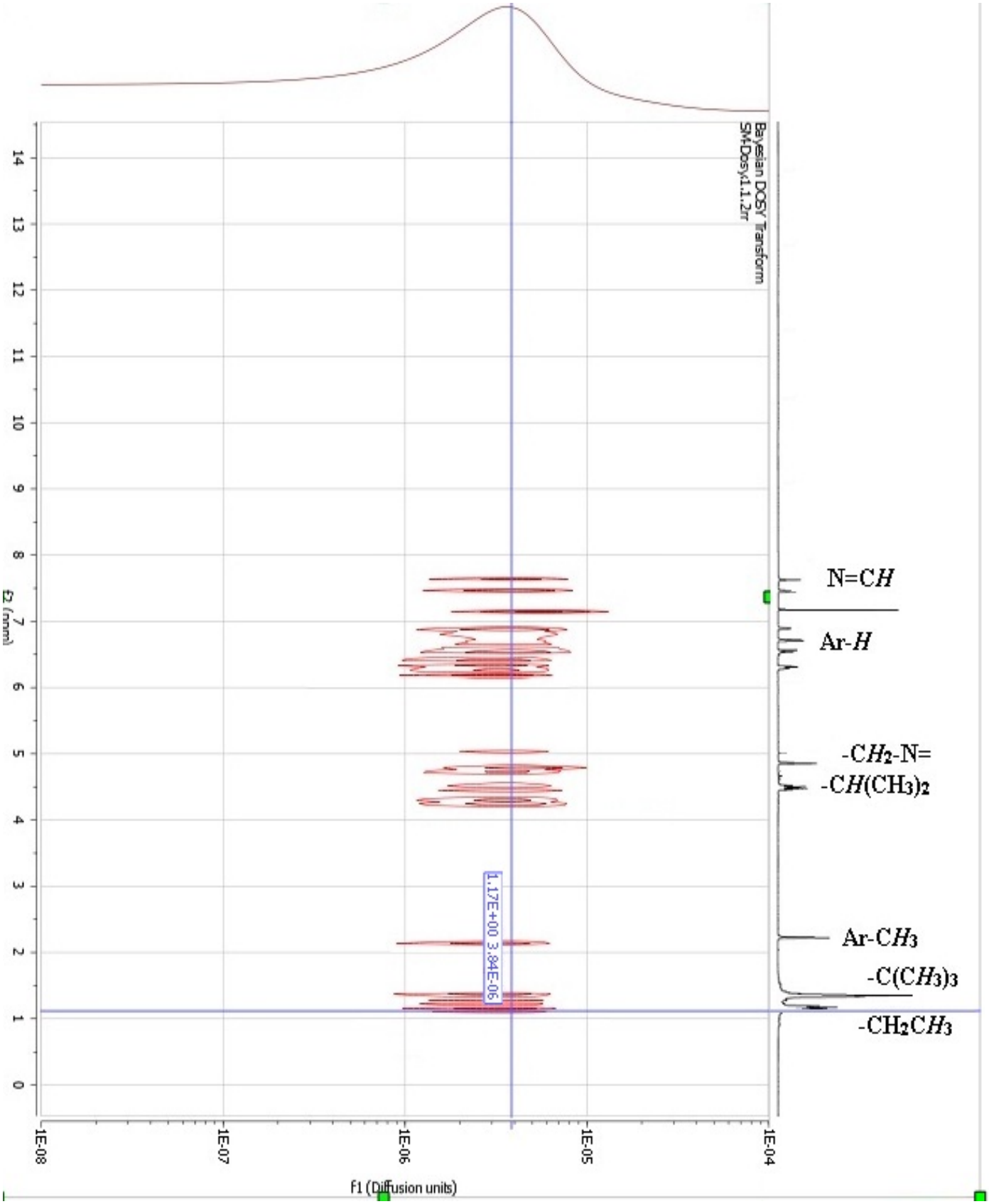

Figure S47. ^{1}H DOSY NMR spectrum of **5a**

General procedure for the calculation of hydrodynamic radius

The hydrodynamic radius of **5a** was calculated from the average diameter (d_{av}) of d_v (vertical), d_h (horizontal) and d_d (diagonal), obtained from the single crystal XRD structure (taking the measurement between the furthest atoms in each case).[1] The R_H value was then correlated with the value obtained from ^{1}H DOSY NMR spectrum.

$R_H = d_{av}/2$, where $d_{av} = (d_v + d_h + d_d)/3$

Although we reported R_H calculated by the above procedure, there is another approach to the calculation. The minimum radius R_{min} can be calculated from the molecular volume determined from www.molinspiration.com by the formula $V_{mol} = (4\pi/3)R_{min}^3$. The maximum distance between the furthest atoms (d_{max}) was obtained from single crystal XRD structure and the maximum radius was determined from d_{max}. The hydrodynamic radius was then calculated from the average of R_{max} and R_{min}.[2] Both the approaches led to almost similar results.

References

1) S. Neogi, Y. Lorenz, M. Engeser, D. Samanta and M. Schmittel, *Inorg. Chem*. 2013, **52**, 6975−6984.

2) L. Azor, C. Bailly, L. Brelot, M. Henry, P. Mobian and S. Dagorne, *Inorg. Chem.*, 2012, **51**, 10876-10883.

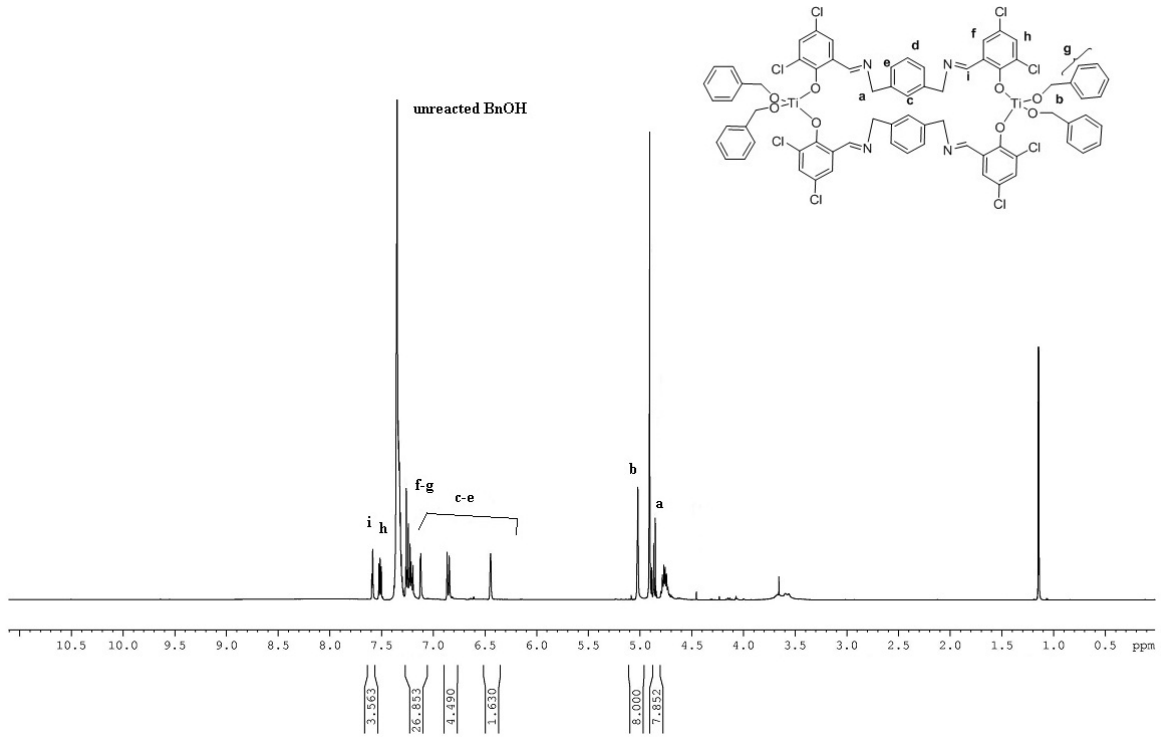

Figure S48. ^{1}H NMR spectrum of **3** in presence of excess BnOH

Table S2. Experimental and calculated ^{1}H and ^{13}C NMR chemical shifts (ppm) of the optimized compound **5a** and **8**

Complex 5a

Entry	Expt. NMR	Calc. Shield	Calc. NMR	Averaged NMR
C1	160.34	24.24	158.25	
C9	166.81	17.00	165.49	
C11	59.91	124.71	57.78	
C41	166.81	18.81	163.65	
C44	160.34	21.82	160.68	
C25	26.97	159.94	22.53	24.24
C29		159.72	22.76	
C33		155.06	27.42	
C64	20.64	163.30	19.18	
C68	59.91	123.28	59.21	
C169	71.13	110.07	69.41	
C172	14.13	168.69	13.78	
H10	7.65	24.53	7.35	
H12	4.70	26.96	4.92	
H13	4.73	26.75	5.13	
H30	1.47	30.48	1.40	1.42
H31		30.47	1.41	
H32		30.44	1.44	
H39	2.17	29.64	2.24	
H42	7.65	24.56	7.42	
H53	1.54	30.43	1.45	1.46
H54		30.42	1.46	
H55		30.40	1.48	
H65	2.23	29.55	2.33	
H69	4.70	26.96	4.92	
H70	4.73	26.75	5.13	
H79	4.20	27.93	3.95	
H82	1.42	30.63	1.25	
H170	4.20	27.93	3.95	
H174	1.42	30.63	1.25	

Complex 8

Entry	Expt. NMR	Calc. Shield	Calc. NMR	Averaged NMR
C10	161.26	23.47	158.99	
C18	60.15	125.25	57.21	
C29	168.27	16.08	165.67	
C68	160.60	24.79	157.67	
C71	167.34	22.92	159.56	
C79	62.40	123.25	59.13	
C143	75.22	108.42	74.05	
C144	33.08	148.61	33.75	33.17
C145		149.94	32.44	
C146		149.06	33.31	
C182	75.25	107.75	74.73	
C183	33.20	148.68	33.57	33.85
C184		148.86	33.52	
C185		147.93	34.45	
C221	35.26	147.44	35.03	
C222	29.96	156.93	25.01	26.75
C223		157.43	25.54	
C224		152.75	29.71	
C235	30.20	153.79	28.59	30.64
C236		152.62	29.78	
C237		148.86	33.54	
C294	20.87	161.68	20.74	
C298	21.73	160.76	21.65	
H91	4.85	27.08	4.83	
H92	4.71	27.41	4.47	
H100	7.66	24.13	7.78	
H117	7.59	24.33	7.56	
H121	4.75	27.18	4.7	
H122	4.49	27.46	4.42	
H212	1.13	31.07	0.63	0.96
H215		30.96	0.96	
H218		30.64	1.28	
H225	1.06	31.06	0.83	0.82
H228		31.11	0.78	
H231		31.05	0.84	
H295	2.12	30.62	2.27	
H305	2.23	29.46	2.41	